

Review

# Long-Term Embrittlement of Ancient Copper and Silver Alloys

Omid Oudbashi <sup>1,\*</sup>  and Russell Wanhill <sup>2,\*</sup> 

<sup>1</sup> Department of Conservation of Cultural and Historical Properties, Art University of Isfahan, P.O. Box 1744, Isfahan 8146834615, Iran

<sup>2</sup> Aerospace Vehicles Division, Royal Netherlands Aerospace Centre, P.O. Box 153, 8300 AD Emmeloord, The Netherlands

\* Correspondence: o.oudbashi@au.ac.ir (O.O.); rjhwanhill@gmail.com (R.W.)

**Abstract:** The manifestations of ancient metals' embrittlement, cracking and fracture, are challenging problems for restorers and conservators, yet the scientific understanding of these problems is limited. In particular, the study and interpretation of fracture surfaces, fractography, is a minor or non-existent consideration for most archaeometallurgical investigations. This paper presents a survey of fractographic analyses, in combination with the more widely used disciplines of microstructural studies, metallography, and chemical analyses for some Old-World copper alloy (bronzes) and high-silver alloy artifacts that have undergone long-term corrosion and embrittlement damage. We show that fractography, as an adjunct to metallography, can improve the interpretation of these types of damage and assist in selecting the best methods for restoration and conservation of the objects made from these alloys.

**Keywords:** copper alloys; high-silver alloys; corrosion; embrittlement; fracture surfaces; fractography; metallography; chemical analysis; restoration; conservation



**Citation:** Oudbashi, O.; Wanhill, R. Long-Term Embrittlement of Ancient Copper and Silver Alloys. *Heritage* **2021**, *4*, 2287–2319. <https://doi.org/10.3390/heritage4030130>

Academic Editor: Chiara Soffritti

Received: 12 August 2021

Accepted: 7 September 2021

Published: 10 September 2021

**Publisher's Note:** MDPI stays neutral with regard to jurisdictional claims in published maps and institutional affiliations.



**Copyright:** © 2021 by the authors. Licensee MDPI, Basel, Switzerland. This article is an open access article distributed under the terms and conditions of the Creative Commons Attribution (CC BY) license (<https://creativecommons.org/licenses/by/4.0/>).

## 1. Introduction

This paper surveys damage, particularly cracking, caused by long-term corrosion-induced embrittlement of ancient copper and silver alloys, as well as long-term, microstructurally induced embrittlement of silver alloys. The emphasis is on fractography, the analysis and interpretation of fracture surfaces, which is, or should be, an important adjunct to microstructural metallographic studies and chemical analyses. The occurrence of cracking and fracture are obviously important for restoration and conservation, yet detailed knowledge of the causes and significance of such damage has rarely been obtained. For example, there are (i) excellent books and symposium proceedings with metallographic and chemical analyses for ancient and historic metals, but no fractography [1–5]; and (ii) authoritative publications on research frameworks and guidelines for best practice that do not mention fractography [6,7]. This situation is partly because metallography has proven to be a powerful diagnostic technique for ancient objects (artifacts and coins); partly because of a general unfamiliarity with fractography; and also because it is difficult to obtain suitable samples that can be broken open to reveal cracking and fracture details. These details would otherwise (except for high-karat gold and platinum-group alloys) be obliterated by centuries and millennia of general corrosion in burial environments.

We have been able to provide several examples (case studies) to improve the appreciation of fractography as a diagnostic technique, as well as the detailed significance of cracking and fracture. With the aid of these examples, and taking relevant ethical considerations into account, the latter part of this paper discusses the actual and potential remedial measures for the restoration and conservation of corroded, cracked, and broken artifacts.

## 2. Corrosion and Embrittlement of Old World Copper Alloy Objects

### 2.1. Production and Processing

Native copper was the first material used to produce artifacts in prehistory. Evidence of native copper use is observed in early metallurgy around the ancient world [8]. Somewhat later, pyrometallurgy was developed to extract copper from oxidic ores. Copper compounds such as malachite ( $\text{CuCO}_3 \cdot \text{Cu}(\text{OH})_2$ ) were smelted in crucibles inside primitive furnaces, and the extracted metallic copper was used to produce small objects by using manufacturing processes such as casting in simple open molds, hammering, or a mixture of both [9]. Further developments enabled the smelting of sulfidic copper ores, a more complicated process, to obtain copper [9,10]. This led to greater amounts of copper to produce larger objects. Contemporaneously developed manufacturing and shaping techniques allowed the metalworkers to make bigger and more complex objects, including large sculptures with complex forms, larger and more functional weapons and tools, as well as decorative artifacts. There is clear evidence that these process developments occurred during the Neolithic and Chalcolithic periods (ca. 7000–3000 BC) in the Old World, i.e., the Near East and Europe [10,11].

The first attempts to improve the physical/mechanical properties of copper were to add other metallic elements to produce early alloys. According to the literature, arsenical copper (Cu-As alloy) was the first copper alloy to appear in ancient times, although early examples are considered to be accidental alloys caused by smelting As-bearing copper ores. Nevertheless, the later arsenical copper objects were made by intentional alloying processes such as direct smelting of polymetallic Cu-As-bearing ores or adding speiss (a mixture of impure metallic arsenides) to copper [12–14].

Another, and the most important, copper alloy was (and is) tin bronze (Cu-Sn). Early evidence of tin bronze objects has been found at the beginning of the so-called Bronze Age (ca. 3000 BC) [15]. Tin bronze was produced by different alloying processes such as co-smelting, cementation, adding metallic tin to metallic copper, or smelting of tin-bearing copper ores [16,17]. These ancient alloys are classified as low-tin (<15 wt.%) and high-tin (>15 wt.%) bronzes, corresponding to single-phase or multiple-phase microstructures, although the formation of other phases is observed in low-tin bronzes owing to non-equilibrium solidification [10].

Copper alloys metallurgy was further developed by adding other elements, notably zinc to produce brasses. The high solubility of zinc in copper allows the production of a single-phase Cu-Zn alloy with a wide variation in zinc content [10]. Brass was made from about 2000 years ago by ancient civilizations such as the Roman Empire [18].

### 2.2. General Corrosion

Ancient and historic copper alloy artifacts show diverse and complicated corrosion behavior in different environments. Many factors affect the rate, mechanisms, and morphology of corrosion in copper alloys, including the chemico-physical conditions of the environment(s), the alloy compositions, and the manufacturing processes [19–21]. Nevertheless, the long-term placement environments (soil, seawater, or outdoor exposure) play dominant roles.

Corrosion of buried copper alloys in soil environments is a complex process leading to the formation of various and variable morphologies with different corrosion products. The artifacts may be covered by a more or less thick layer consisting of corrosion/oxidation products, or they may be corroded completely into a multi-layered bulk material without any remaining metal [21,22]. In alkaline soils, a thin layer of cuprite ( $\text{Cu}_2\text{O}$ ) may be formed over the metal, on top of which there may be a significant layer of malachite ( $\text{Cu}_2\text{CO}_3(\text{OH})_2$ ). Malachite (or basic copper carbonate) is formed by the reaction between copper/copper oxides and carbonate/bicarbonate anions dissolved in soil water, leading to the formation of a green patina [21,23]. Other possibilities are (i) azurite ( $\text{Cu}_3(\text{CO}_3)_2(\text{OH})_2$ ), an isomer of malachite, a rare corrosion product that has been reported for some buried copper alloys [23]; and (ii) the presence of chloride ions in the soil may lead to the formation

of nantokite ( $\text{CuCl}$ ), which forms the copper trihydroxychlorides atacamite or paratacamite ( $\text{Cu}_2(\text{OH})_3\text{Cl}$ ) in the presence of moisture and oxygen. This latter corrosion process is called “Bronze Disease”. It is a cyclic reaction caused by transformation of nantokite to trihydroxychlorides and continues until all the copper is transformed into copper corrosion products [21,22,24].

Corrosion of copper alloys in (deep) seawater tends to be more anaerobic owing to the lower oxygen concentration at depths below about 10 m. The corrosion is also influenced by an interplay between the toxicity of the copper corrosion products and growth of microorganisms on the metal surface [21,25]. Various corrosion products form, including oxygen-bearing copper oxides and trihydroxychlorides as well as sulfides. The formation of these compounds strongly depends on the oxygen content of the seawater: At shallow depths (aerobic), the first group of corrosion products forms; in deeper water (anaerobic), the second group is the main corrosion products. The copper sulfides are due to the activity of sulfate-reducing bacteria (SRB) [21,26,27].

Corrosion of copper-based artifacts exposed to the outdoor environment depends on the types and concentrations of atmospheric pollutants. In today’s world, the corrosion products are different for urban, rural, and seaside environments [21]. In urban environments, basic copper sulfates such as brochantite, antlerite, and posnjakite are commonplace corrosion products, together with cuprite; while in rural regions, copper oxides and carbonates are the main corrosion products [28]. Copper trihydroxychlorides are observed on some corroded copper-based statues located near the sea [21,28]. These variations show that the main factors determining the corrosion of copper-based objects in outdoor environments are the presence and concentration of gaseous and particulate pollutants such as  $\text{SO}_x$ ,  $\text{NO}_x$ ,  $\text{CO}_2$ , dust, and salt spray from the sea [21]. N.B.: This summary is not necessarily, or even at all, applicable to ancient urban environments, which would be largely or entirely free of today’s industrial pollutants.

### 2.3. Alloying Element Influences on Corrosion

As noted in Section 2.2, copper alloy corrosion varies in different environments. Unalloyed copper corrodes via oxidation, dissolution, and re-deposition of copper ions, leading to the formation of a cuprite patina and copper II corrosion products: Atacamite and paratacamite ( $\text{Cu}_2\text{Cl}(\text{OH})_3$ ), brochantite ( $\text{Cu}_4\text{SO}_4(\text{OH})_6$ ), posnjakite ( $\text{Cu}_4\text{SO}_4(\text{OH})_6 \cdot \text{H}_2\text{O}$ ), malachite ( $\text{Cu}_2\text{CO}_3(\text{OH})_2$ ), and gerhardite ( $\text{Cu}_2\text{NO}_3(\text{OH})_3$ ) [21]. The types and compositions of Cu II products strongly depend on the environment [20,22]. Copper alloys, e.g., Cu-As, Cu-Zn, and Cu-Sn alloys, exhibit more complex and interesting corrosion features due to different reactions of the constituent metallic elements with the environments.

#### 2.3.1. Arsenical Copper Alloys (Cu-As)

The corrosion of arsenical copper (arsenical bronze) objects has not been investigated sufficiently in detail to obtain definitive conclusions about the mechanisms of corrosion and morphologies of the corrosion products. However, the presence of arsenic as an alloying element may lead to some resistance against corrosion during long-term burial, and also decrease the corrosion rate [21]. It is worth noting that a specific corrosion morphology due to arsenic has not been reported. N.B.: A silvery appearance is observed in some ancient Cu-As objects, and this has been attributed to different causes: Inverse segregation, cementation, or corrosion (probably artificially initiated corrosion) [29–31]. This phenomenon is not well understood and is under investigation.

#### 2.3.2. Brass Alloys (Cu-Zn)

The most well-known corrosion process in brasses is dezincification [32,33]. This occurs due to selective dissolution (leaching) of zinc during corrosion, whereby zinc is lost and copper is left behind, leading to the formation of a copper-rich surface [34]. This is a type of de-alloying due to the loss of the more reactive component (zinc) from the alloy [35].

The main corrosion products from Cu-Zn alloys are similar to those for unalloyed copper objects, although some evidence of zinc corrosion products may be observed [36,37].

### 2.3.3. Bronze Alloys (Cu-Sn)

The presence of tin in bronze objects results in some interesting features of their corrosion mechanisms and corrosion product morphologies. In fact, the main difference between the corrosion morphologies of other copper alloys and tin bronzes is due to the behavior of tin during corrosion [21]. The main corrosion mechanism in ancient bronzes (in all natural environments) is selective dissolution of copper and internal oxidation of tin [38–40]. This process is also generally independent of the manufacturing techniques of objects, although some variations are visible on a microscopic scale, namely whether the microstructure is dendritic (castings) or worked and annealed [38,39,41].

The metallographic literature enables the identification of two main corrosion morphologies for archaeological tin bronze objects [38,42,43]. The first, type I corrosion, is a two-layered corrosion structure consisting of:

- An external layer with variable thickness on the same object and on different objects. This layer consists of powdery minerals that include basic copper carbonates, malachite, and azurite, together with some soil minerals or contamination materials.
- An internal layer below the original surface. This layer is tin-rich relative to the bulk metal, compact, and green/blue/grey in color, and may retain evidence of the original alloy's microstructure and inclusions (secondary phase particles).

This corrosion morphology occurs in tin bronze objects exposed to non-corrosive or moderately corrosive environments such as low-chloride burial soil, freshwater, or rural atmospheric environments [39,41,44,45].

The second corrosion morphology, type II, is observed on objects buried in or exposed to chloride-contaminated environments for long periods [38,46]. This is a three-layered corrosion structure consisting of:

- An external layer with variable thickness on the same object and on different objects. This layer consists of powdery minerals that include basic copper chlorides.
- A thick red layer of copper oxide that contains the original surface, although this is not *visibly* detectable.
- An internal corrosion layer below the original surface that is tin-rich relative to the bulk metal. In some cases, all of the bulk metal has been transformed to corrosion products.

The formation of internal tin-rich corrosion layers for both corrosion types is due to selective dissolution of copper during long-term burial or exposure in corrosive environments, and internal oxidation of tin [38,47,48]. In more detail, (i) the dissolved copper ions migrate to the external surface and react with available anions to form different copper II corrosion products [38,40]; and (ii) oxidation of the tin-rich internal layer retains 'ghost structure' remnants of the original tin bronze microstructure [38–40,46]. The 'ghost structure' is more visible in type I corrosion layers owing to a very low rate of corrosion. However, 'ghost structures' have been observed in type II corrosion layers [38]. Another difference between type I and type II corrosion is the corrosion crust thicknesses. In type I corrosion, the crust thickness is thin, rarely more than 100 µm. However, type II corrosion is generally much thicker and can even consume the entire object [46], as mentioned above.

Another interesting aspect of tin bronze corrosion is the formation of a very thin layer of corrosion along the metal-corrosion interfaces for both types of corrosion. This layer resembles localized intergranular or transgranular corrosion (see Section 2.3.2) but its color is mostly red. This thin red layer represents the early stages of corrosion/oxidation of copper caused by a corrosive solution penetrating into the metal. If this becomes extensive, this localized corrosion may result in cracking and embrittlement of archaeological tin bronzes, especially if they retain large amounts of deformation in the microstructure [38–40].

#### 2.4. General Corrosion

Some examples of general corrosion of archaeological copper alloys will be discussed in the following subsections.

##### 2.4.1. Tin Bronze Luristan Coffin, 6th–10th Centuries BC

The coffin, with contents, is shown in Figure 1. It was discovered in Western Iran (Luristan), had broken into large pieces, and was covered with a thick layer of green corrosion products mixed with soil. Inductively coupled plasma–mass spectroscopy (ICP-MS) analysis determined that the alloy composition is 90.32 wt.% Cu, 8.23 wt.% Sn, 0.39 wt.% Pb, 0.30 wt.% P, 0.24 wt.% As, and 0.13 wt.% Fe. Metallography showed that the coffin has a worked and annealed grain microstructure in which remnants of coring (left over from initial casting) were visible as parallel bands in etched samples. These details demonstrated that the working and annealing process was insufficient to remove all of the initial coring [49].



**Figure 1.** Bronze coffin from Luristan, Iran. *Original images with permission: Falak-ol-Aflak Museum, Khorramabad.*

The corrosion occurring during burial was studied by scanning electron microscopy with energy dispersive analysis of X-rays (SEM-EDS). Figure 2 shows SEM backscattered electron (BSE) metallographic cross-sections. These have a two-layered morphology consisting of an external layer (A) and internal layer (B), with some remnants of a metallic structure (M), as seen in Figure 2a. Furthermore, significant intergranular corrosion attack is visible in the metallic structure at the higher magnification, as shown in Figure 2b.

EDS analyses of these layers are presented in Table 1. The metallic structure (M) has a composition typical of tin bronze, as was shown by the ICP-MS analysis. Note that the internal corrosion layer (B) shows a higher Sn/Cu proportion than the metallic structure, i.e., the internal layer has been enriched in tin. On the other hand, the external layer (A), formed over the original surface, has a very low tin concentration compared to the M and B locations.

The morphology and chemistry of the corrosion layers suggest, on the whole, that the coffin represents type I corrosion. However, while the internal corrosion layer is composed of Cu, Sn, and O, consistent with type I corrosion, the external corrosion layer is composed of Cu, O, and Cl, which is more relatable to type II corrosion. A high concentration of Cl in the external corrosion layer, besides Cu and O, can be attributed to basic copper chlorides (copper trihydroxychlorides) such as atacamite and paratacamite [50]. These have formed a pale green patina on the coffin surface.

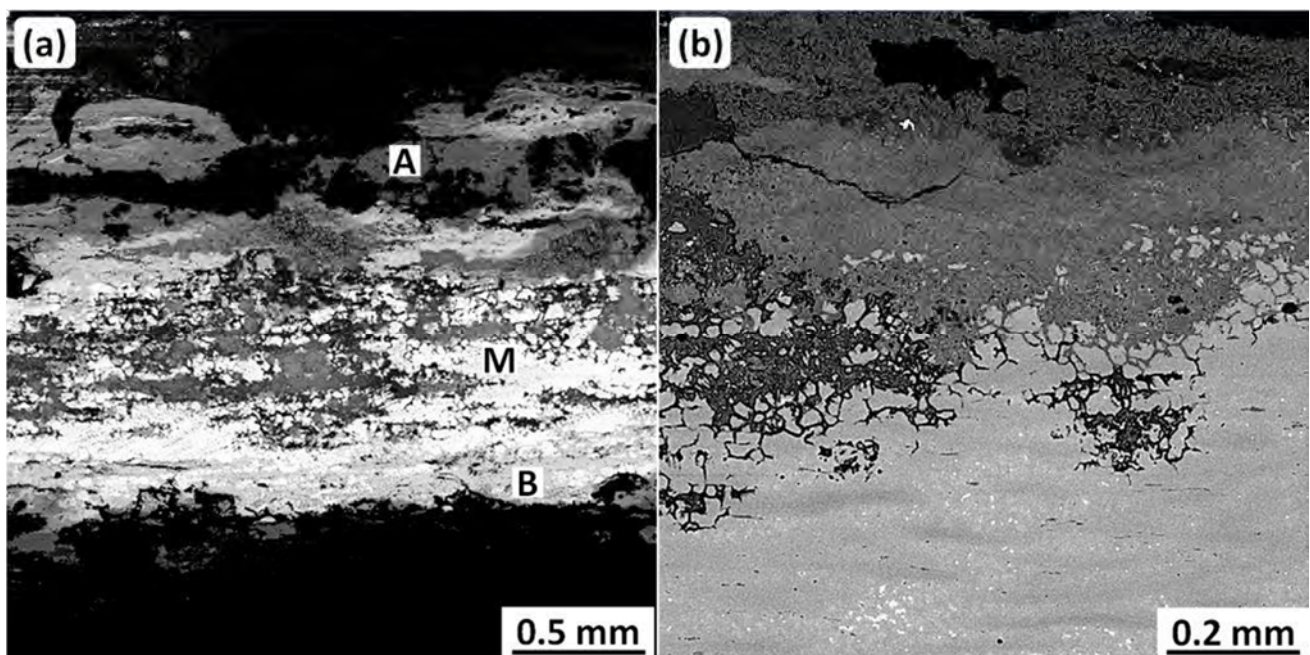


**Figure 2.** SEM-BSE micrographs of sample cross-sections from the Luristan coffin. (a) shows two corrosion layers: External (A) and internal (B); and also the remains of the original metal. (b) shows significant intergranular attack in the remains of the metal. Original images: Omid Oudbashi.

**Table 1.** EDS results from a metallographic sample of the Luristan Coffin, wt.%.

	Cu	Zn	As	Sn	Pb	O	Al	Cl	S	Zn
<b>M</b>	90.66	0.90	2.68	5.74	0.01	-	-	-	-	0.90
<b>A</b>	63.05	-	-	0.69	-	16.46	0.54	19.25	-	-
<b>B</b>	67.96	-	-	15.09	0.59	16.19	-	0.08	0.09	-

As mentioned earlier, according to the literature, type I corrosion occurs in tin bronzes buried in non-corrosive or moderately corrosive environments. These have very low soluble Cl contents that allow the formation of basic copper carbonates (e.g., malachite) on the external surfaces [38,40]. Clearly, the morphology and chemistry of the corrosion layers on the coffin cannot be simply explained as due to type I or type II corrosion.

To resolve this issue, it is suggested that the coffin has undergone type I corrosion that transitioned to an early stage of type II corrosion in which “Bronze disease” (discussed in Section 2.2) has been occurring.

#### 2.4.2. Copper Object (Rod) from Southwestern Iran, ca. 14th Century BC

Figure 3a shows a small rod excavated from Haft Tappeh, Southwestern Iran. The rod was disinterred from a Cl-rich corrosive soil in which all buried copper-based objects had suffered bronze disease [24]: Most had been transformed completely to corrosion products [51]. Nevertheless, a few objects, including the rod, retained some metallic structure. This is illustrated in Figure 3b,c, which shows an optical metallographic cross-section and an SEM metallograph used for EDS analysis.

**Table 2.** EDS analyses from the cross-section of the copper rod, wt.%.

	Cu	Sn	O	Cl	Mg	Si	Al	Ca	K
<b>M</b>	99.77	0.23	-	-	-	-	-	-	-
<b>A</b>	54.59	-	30.77	9.26	0.56	4.02	0.34	0.38	0.09
<b>B</b>	85.78	-	13.66	0.56	-	-	-	-	-

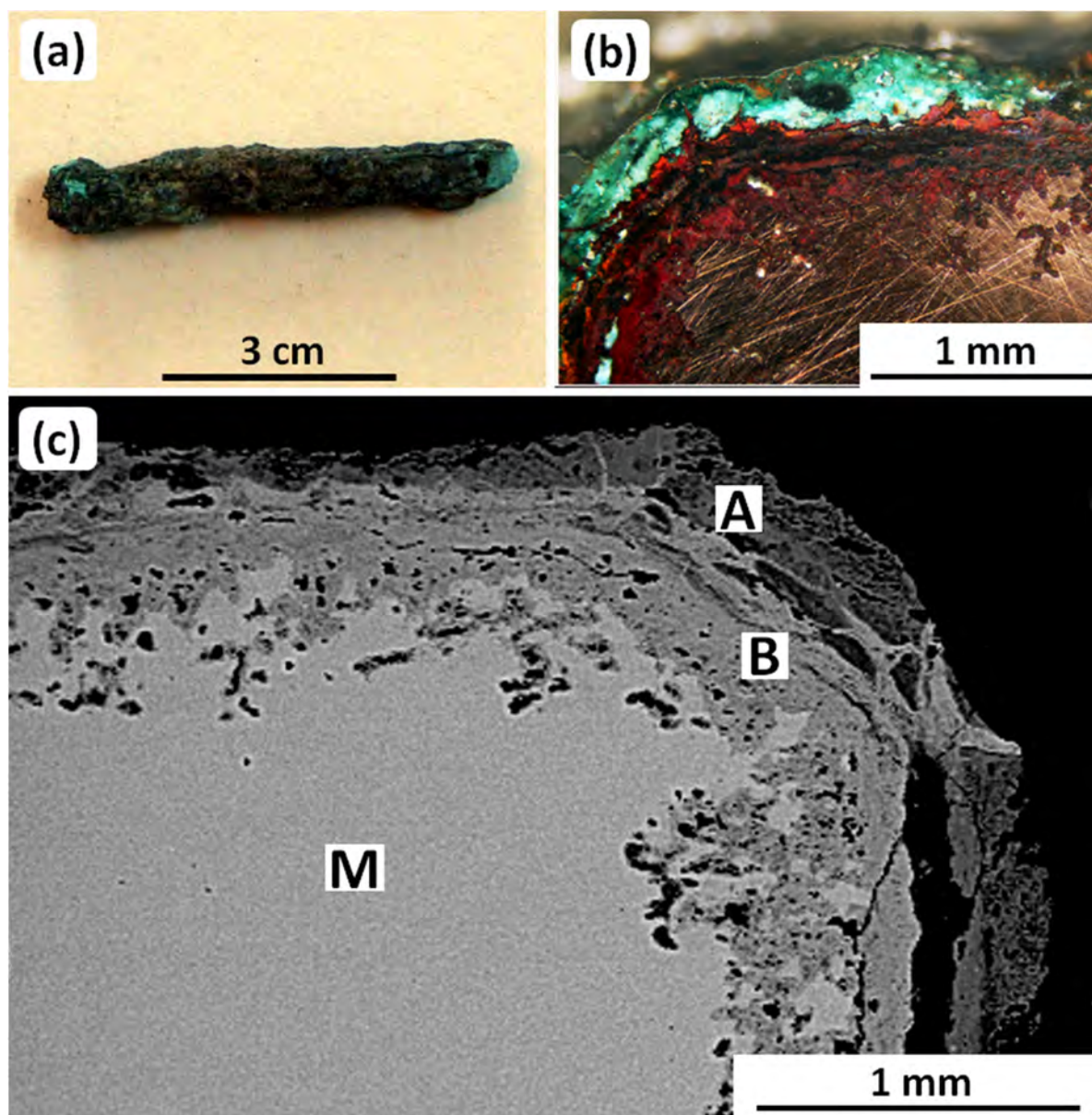


**Figure 3.** (a) The copper-based rod from Haft Tappeh, southwestern Iran, (b) metallographic image of corrosion layers formed on the surface of the rod, and (c) SEM-BSE micrograph showing EDS analysis locations for the metal matrix and corrosion layers; see Table 2 and the main text. *Original images:* Omid Oudbashi.

The EDS analyses are given in Table 2. The analysis of the metallic matrix, M, shows that the rod was made of 99.77 wt.% Cu and 0.23 wt.% Sn, i.e., unalloyed copper. Furthermore, EDS analyses of the internal and external corrosion layers (B and C, respectively) show that the internal corrosion layer is formed by copper oxides, while the external corrosion layer mainly consists of basic copper chlorides. These corrosion products are typical for the bronze objects excavated from the site [46,51].

Metallographic observations on the unetched cross-section of the rod showed no evidence of intergranular corrosion attack, although some pitting was visible under the internal corrosion layer. In addition, the etched cross-section showed that the rod had been shaped by forging with subsequent annealing. Finally, although the rod had been buried in very corrosive soil and therefore was attacked by “Bronze Disease”, the corrosion rate must have been very slow for so much of the metal matrix to have remained.

### 2.4.3. A Bronze Age Low-Arsenic Copper Dagger, 3rd Millennium BC

The dagger was excavated from a small Bronze Age settlement in Southwestern Iran. Figure 4 shows the dagger, which was corroded but intact. Chemical analysis by SEM-EDS showed that the dagger is a low-arsenic copper alloy containing 1.19 wt.% As and 1.92 wt.% Pb, as seen in Table 3.



Figure 4. The Bronze Age dagger from Southwestern Iran. *Original image*: Omid Oudbashi.

Table 3. EDS analyses from the cross-section of the low-arsenic copper dagger, wt.%; see Figure 5 also.

	O	Mg	Al	Si	P	S	Cl	K	Fe	Ni	Cu	Zn	As	Sn	Sb	Pb
Matrix (M)	-	-	-	-	0.05	0.58	0.14	-	0.32	0.30	93.75	0.94	1.19	0.28	0.52	1.92
A	18.91	-	-	-	-	1.08	0.13	-	0.20	0.50	75.87	1.21	0.63	0.18	0.28	1.01
B	54.31	-	-	15.39	0.06	-	0.12	-	0.41	0.39	25.90	0.85	0.59	0.52	0.64	0.81
C	60.46	3.28	6.73	16.88	0.13	0.11	0.13	1.02	3.46	0.82	5.28	1.10	0.33	-	-	0.26

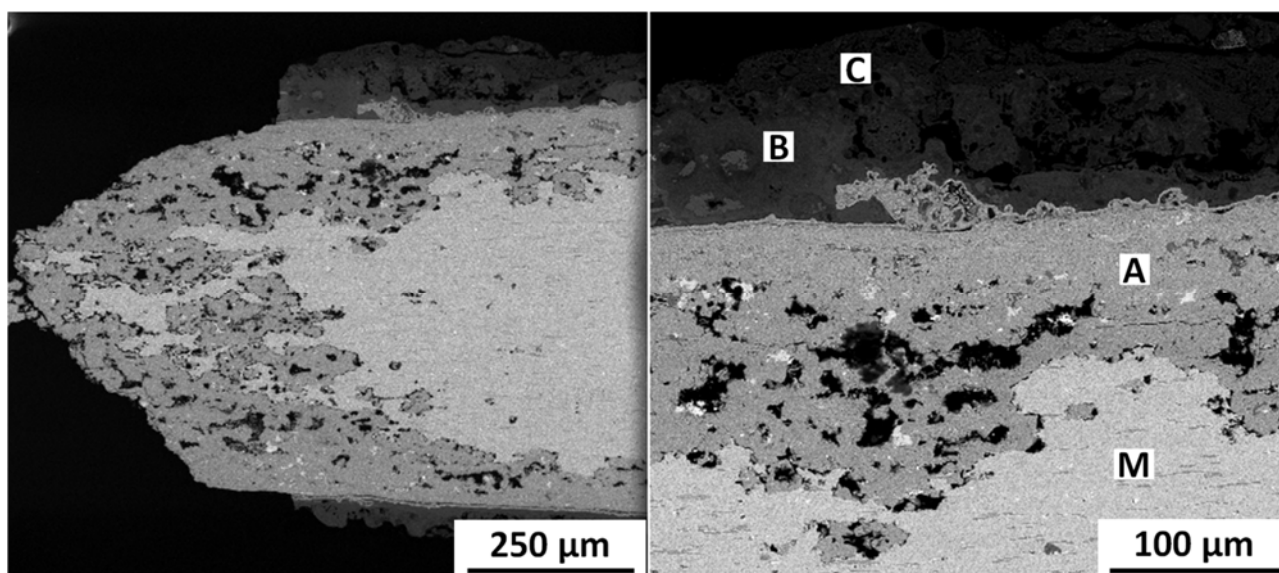


Figure 5. SEM-BSE micrographs from the dagger cross-section, showing the surface corrosion layers. *Original images*: Omid Oudbashi.

The SEM-BSE micrographs from which the analyses were obtained are presented in Figure 5. The micrographs show a variably thick corrosion crust. The original dagger surface is preserved between the corrosion layers A (internal) and B + C (external). The internal layer includes copper (75.87 wt.%) and oxygen (18.91 wt.%), while the arsenic and lead contents are present in lower concentrations than in the matrix. All three corrosion layers contain only low concentrations of chlorine, thereby providing the main reason that

the dagger has a protective patina and did not fragment or corrode completely. In other words, the dagger has undergone type I corrosion.

#### 2.4.4. Tin Bronze Vessel from Luristan, 7th–8th Century BC

A fragmented thin-walled vessel excavated from the Iron Age site of Sangtarashan, in Western Iran (Luristan), has been found to have several interesting aspects. These are uniform surface corrosion and a noble patina [40]; and stress corrosion cracking (SCC) [52], which is discussed in Section 2.5. Figure 6 shows how seriously the vessel had broken into fragments, most probably during excavation.

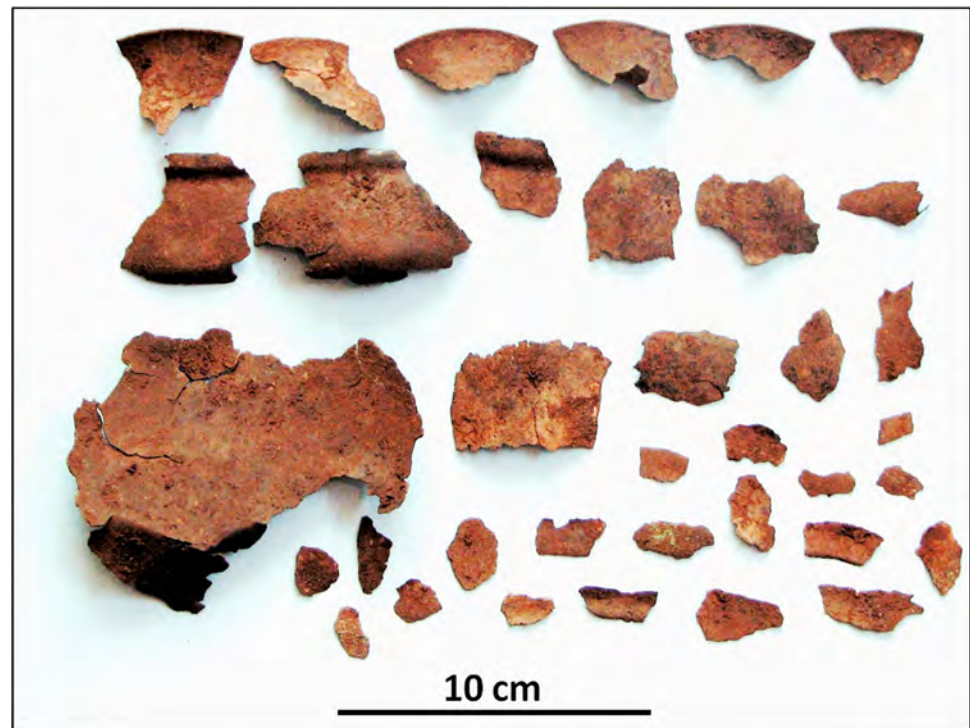


**Figure 6.** The broken vessel excavated from the Sangtarashan Iron Age site, Western Iran. *Original image:* Omid Oudbashi.

The corrosion occurring during burial was studied by optical metallography and SEM-EDS metallography as seen in Figure 7 and Table 4. The results revealed an internal two-layer crust consisting of a 100–200- $\mu\text{m}$ -thick smooth patina, layer **A**, and a region with localized intergranular and transgranular attack, layer **B**. The EDS results showed that (i) the vessel is a binary Cu-Sn alloy, (ii) layer **A** is a tin-rich noble patina with considerable oxygen content owing to tin oxidation, and (iii) the layer **B** tin content was slightly higher than that of the metal matrix (not indicated in Figure 7).

The transgranular attack in layer **B**, shown most clearly in Figure 7a,b, occurred along slip planes. This corrosion-induced visibility of slip therefore indicates some retained deformation after final annealing.

Finally, X-ray diffraction (XRD) chemical analysis identified copper oxides and basic copper carbonates as the main corrosion products formed over the surface of the vessel and other tin bronze objects at this site [40]. These results confirm that type I corrosion, with the formation of a tin-rich noble patina, was typical for this site. Consequently, the corrosion rate was low, persisting for nearly 3000 years of burial time.

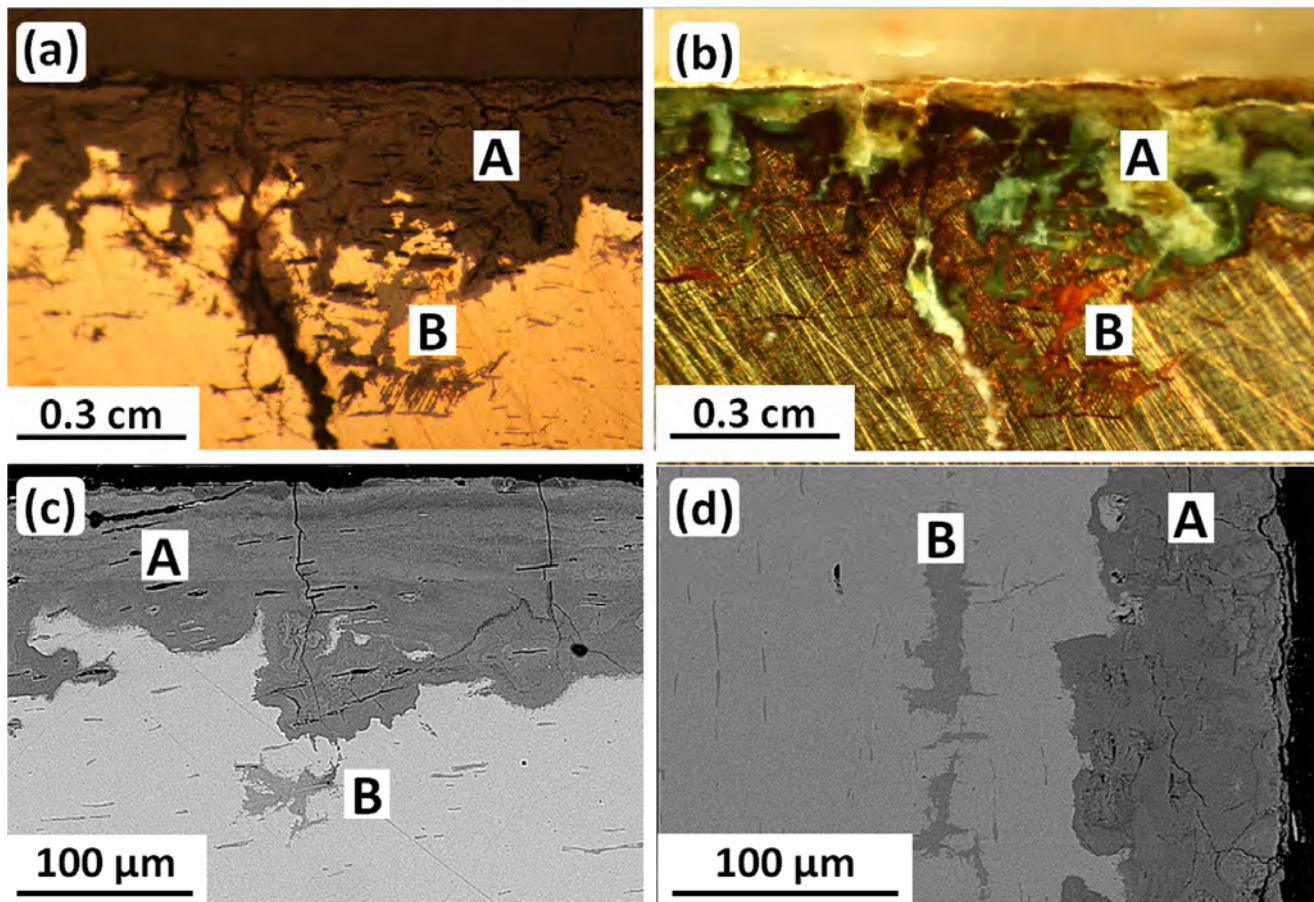


**Figure 7.** Metallography and SEM-BSE micrographs of a cross-section of the tin bronze Luristan vessel. All four images (a–d) show the tin-rich noble patina A and the corrosion attacks in layer B. (a,b) show intergranular and transgranular attack along slip planes in the layer B. Original images: Omid Oudbashi.

**Table 4.** EDS results of phases analyzed from the cross-section of the Sangtarashan bronze vessel, wt.%.

	Cu	Sn	Pb	As	Zn	Ni	Fe	Cl	O	S	P	Si	Ca
<b>Matrix</b>	84.88	13.36	1.16	0.22	0.02	0.01	0.01	-	-	0.15	0.20	-	-
<b>A</b>	10.77	42.02	0.43	0.05	-	-	-	0.04	42.98	-	1.20	1.69	0.81
<b>B</b>	54.82	19.74	0.78	-	-	-	-	1.31	22.76	-	0.59	-	-

### 2.5. Selective Corrosion: Stress Corrosion Cracking (SCC)

As is evident from the examples presented in Section 2.4, ancient bronze objects are highly susceptible to corrosion. This includes selective corrosion owing to stress corrosion cracking (SCC). We have obtained evidence for SCC mainly from metallography, and also, with difficulty, from fracture surfaces (fractography). This is because naturally occurring fracture surfaces during burial are corroded beyond recognition. Instead, some samples have been broken open in the laboratory for SEM fractography [52].

#### 2.5.1. Metallography of Ancient Bronze SCC

Examples of SCC in ancient Iranian bronzes are shown in Figure 8, and their details are given in Table 5. It is evident that severe intergranular attack can lead to breakages.

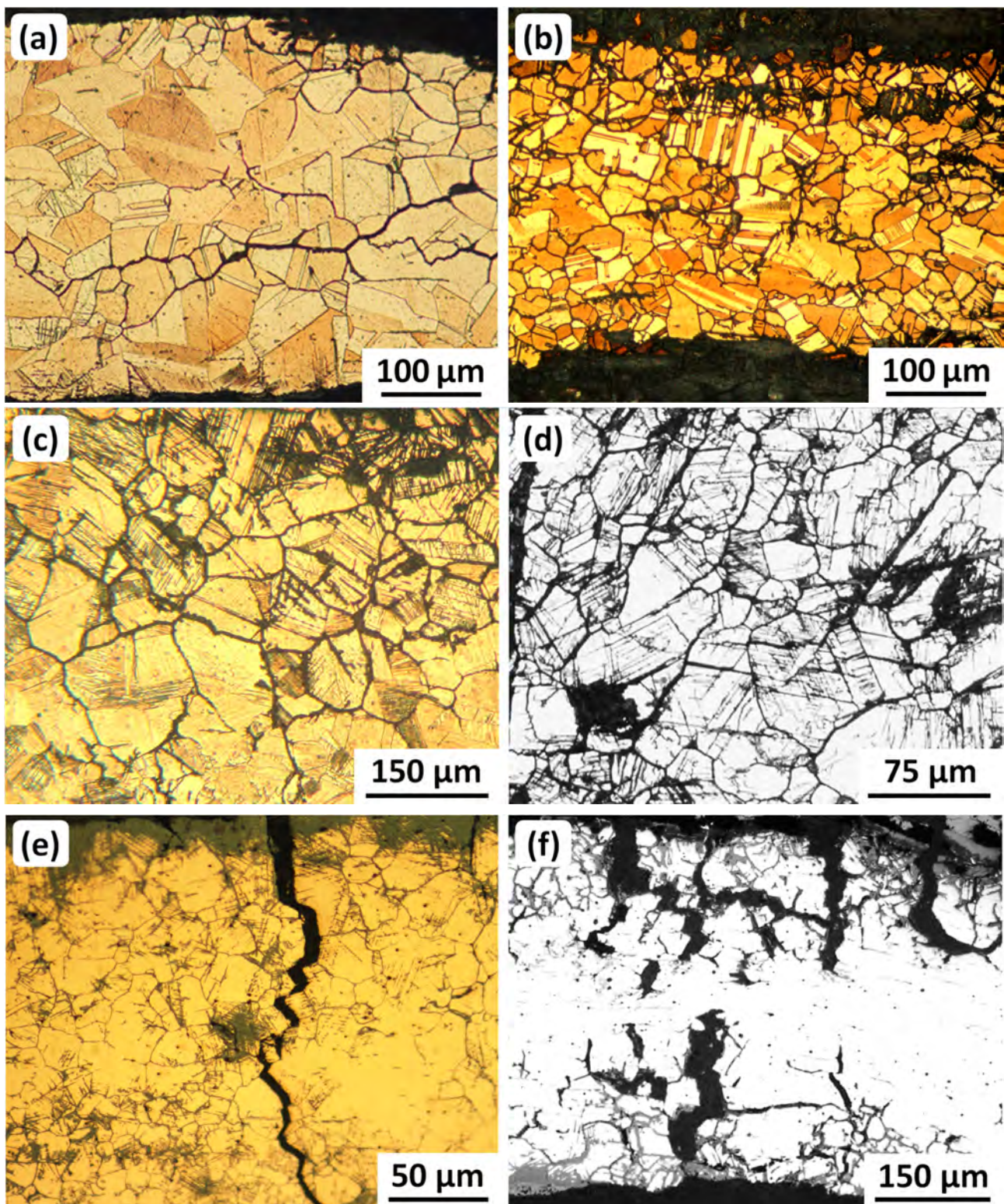


**Figure 8.** Metallographic examples of progressive SCC damage in ancient Iranian bronzes. All six images (a–f) show intergranular cracking. (b) shows some attack along twin boundaries; and (c–e) show attack along twin boundaries and slip lines. More details about the samples are given in Table 5. Original images with permission: (a–c,e) Omid Oudbashi; (d,f) George Vander Voort, Vander Voort Consulting LLC, Wadsworth, IL 60083-9293, USA.

**Table 5.** Details of Iranian ancient bronze metallographic samples shown in Figure 8.

Figure	Artifact: Location: BC Date	Composition (wt.%)	Remarks
Figure 8a	Vessel: Marlik: 10th–14th Century	Cu-8.71Sn-0.02As-0.12Zn	Intergranular cracking
Figure 8b	Vessel: Deh Dumen: 20th–25th Century	Cu-7.69Sn-0.23As-0.12Zn	Intergranular cracking and some attack along twin boundaries
Figure 8c	Vessel: Deh Dumen: 20th–25th Century	Cu-8.41Sn-0.11As-0.12Zn-0.11Pb	Intergranular cracking and attack along slip lines and twin boundaries: large intergranular crack in (e)
Figure 8d	Vessel: Luristan: 7th–8th Century	Cu-18.2Sn-0.06As	
Figure 8e	Button: Baba Jilan: 8th Century	Cu-8.41Sn-0.42As-0.09Zn-0.31Pb	
Figure 8f	Vessel: Luristan: 7th–8th Century	Cu-9.5Sn-0.33As	Large intergranular cracks

### 2.5.2. Fractography of Ancient Bronze SCC

Fractographic examination of gold-coated (needed for SEM imaging) samples from six cracked and fragmented Iranian ancient bronze vessels showed that most of the fracture surfaces were too corroded to determine any SCC characteristics. However, samples from a Baba Jilan vessel (8th Century BC) and the Sangtarashan vessel (7th–8th Century BC) discussed in Section 2.4.4 enabled both intergranular and transgranular SCC to be observed, as shown in Figure 9.

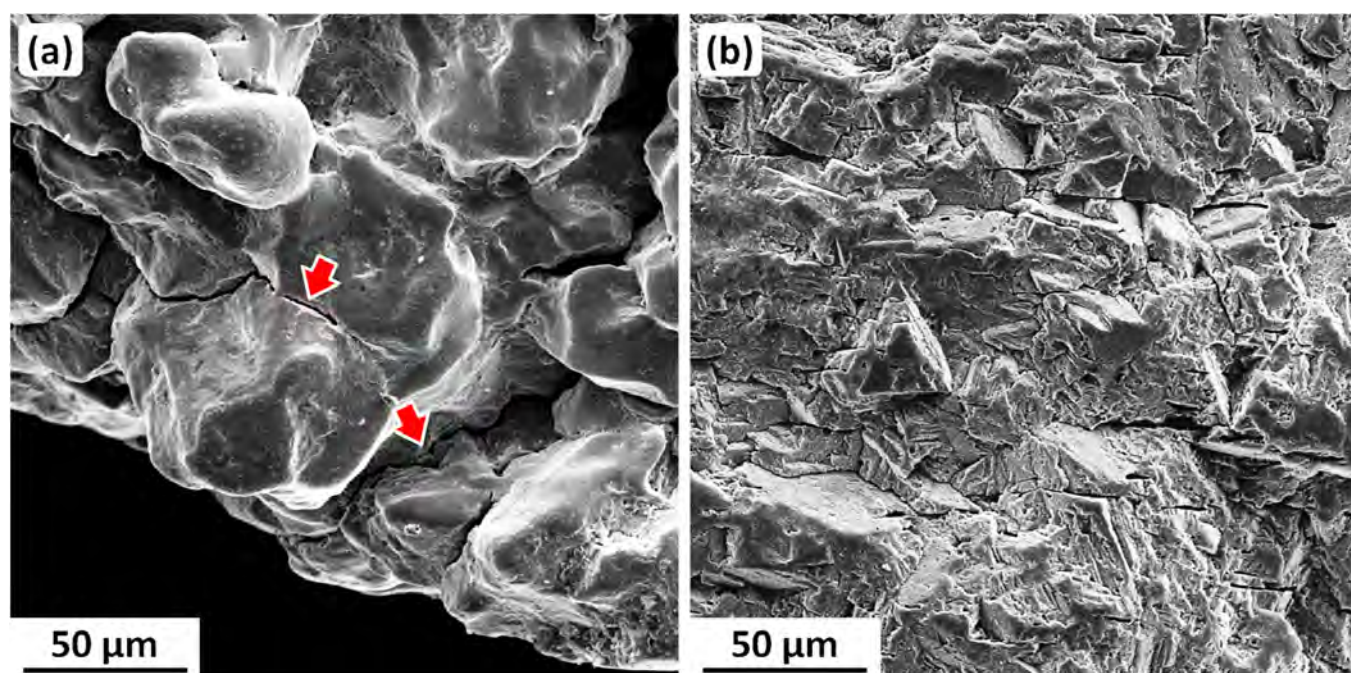


**Figure 9.** SEM secondary electron (SE) fractographs from broken-open fragments of two ancient Iranian bronze vessels: (a) Baba Jilan (8th Century BC) showing intergranular SCC, with two arrows pointing to cracking and spalling of a thin corrosion layer overlying the fracture surface; (b) Sangtarashan (7th–8th Century BC) showing crystallographic transgranular SCC along many slip planes and possibly some annealing twin boundaries. *Original images:* Omid Oudbashi.

## 3. Corrosion and Embrittlement of Old World High-Silver Objects

### 3.1. Production and Processing

Native silver was, and is, scarce, and has seldom been used for artifacts, some of which have recently been dated to as early as 4300–4000 BC [53]. The main source of silver is as a minor component in the ores of other metals, notably lead [54]. Sometime before 3000 BC, in the near- and middle-East, lead obtained from smelting argentiferous lead

ores was further processed by cupellation [55,56] to extract silver. This process became the primary method of obtaining silver for the manufacture of silver objects [57–61], although some were made from silver obtained via direct smelting of silver ores [54].

Cupellation produces silver above 95 wt.% purity [60,62], though it usually contains minor-to-trace amounts of gold, copper, bismuth, and lead (generally below 1 wt.% for each), and traces of antimony, arsenic, tellurium, zinc, and nickel [58,61,63]. Several studies have shown that copper contents above 0.5–1 wt.% indicate deliberate additions [58,63], most probably to increase the strength and wear resistance in high-silver alloys, and also in larger amounts to make lower-quality artifacts and coins. Copper additions appear to have been conducted since about 3000 BC [58].

Aggregations of cupelled silver ‘buttons’, with or without additions of copper, were remelted into ingots. The ingots were used to manufacture artifacts and coinage. Artifacts were usually made by cold working with intermittent annealing, although cast silver objects were also produced. The artifacts were often high-quality thin-walled vessels with exquisite craftsmanship and raised or chased designs. Most coins were made by casting blanks and then striking (hammering) them between dies, although some were cast directly to shape in molds.

### 3.2. General Corrosion

General corrosion in high-silver artifacts and coins is the slow conversion of the metal surface to silver chloride [57,64,65]. The silver chloride forms a moderately cohesive finely granular crust under which the original surface topography may be retained [64]. However, unfavorable conditions can result in an object being completely converted to silver chloride, sometimes retaining its shape, sometimes not [57,64].

### 3.3. Selective Corrosion: Stress Corrosion Cracking (SCC)

Selective corrosion penetrates the metal along preferred paths, reducing an object’s resistance to fragmentation [66–70]. There are three types: (i) Intergranular corrosion in mechanically worked and annealed objects; (ii) interdendritic corrosion in cast objects [65]; and (iii) both intergranular and transgranular corrosion in objects retaining significant amounts of cold work in the finished condition [71,72]. In fact, the study of six corrosion-embrittled artifacts of widely varying dates and provenance [72] has recently led to the conclusion that both intergranular and transgranular corrosion, and the ensuing embrittlement, are due to stress corrosion cracking (SCC). Three examples will be discussed in the following three Sections 3.3.1–3.3.3.

#### 3.3.1. Romanesque Kaptorga (Amulet and Relic Container), AD 10th Century

The Kaptorga is shown in Figure 10. It took more than a year to restore, and this is nonreversible owing to the Kaptorga’s fragility. The bulk composition, determined by EDX/EDS, is 94–95 wt.% Ag, 3.3–3.5 wt.% Cu, and 2.3–2.5 wt.% Au [69]. The Kaptorga has a fully annealed and therefore nominally stress-free microstructure [69], and should have been immune to SCC. However, it was originally (and now after restoration) a hollow, thin-walled object. Thus, during burial, the soil pressing down on it would have introduced bending stresses in the side surfaces. The tensile components of these stresses, amplified by some grooves in the external decorations, must have enabled localized SCC to occur. Figure 11 shows SEM images that illustrate (a) corrosion pitting at grain boundaries, linking to form SCC cracks, and (b) an intergranular SCC fracture that was being slowly destroyed by general corrosion proceeding inwards from a side surface [72].

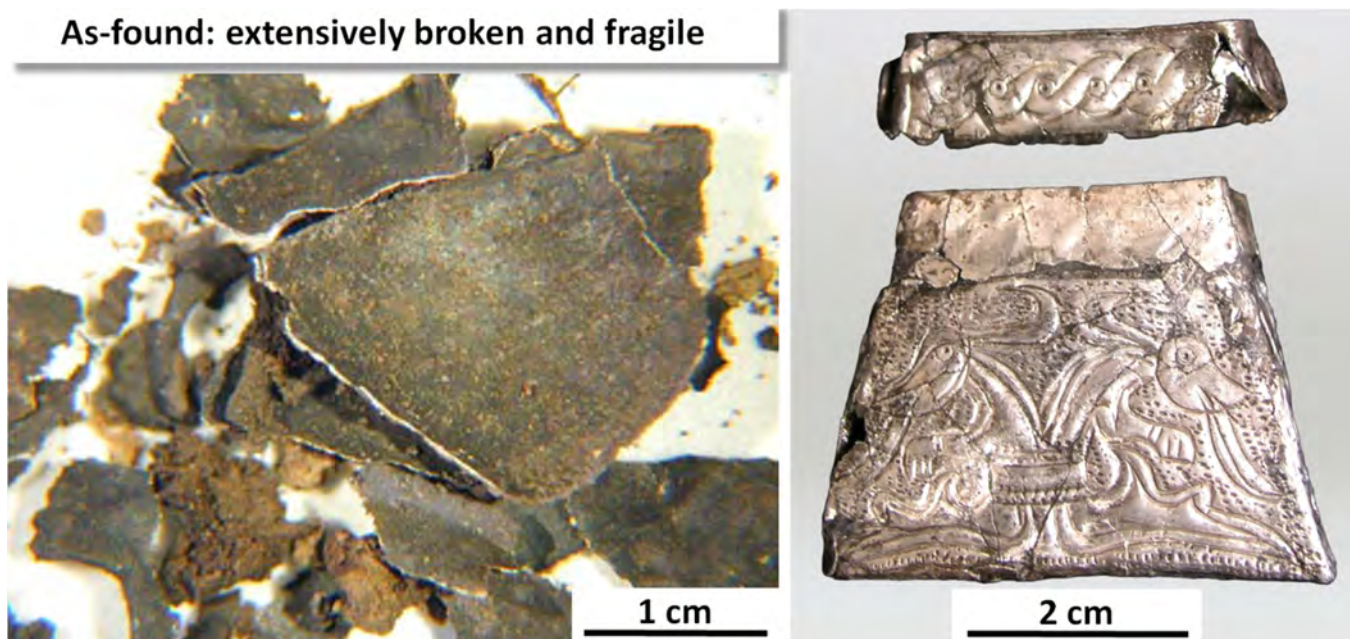


**Figure 10.** The Kaptorga in the as-found condition and restored. *Original images with permission: Jiří Děd, Institute of Chemical Technology; Institute of Archaeology of the Czech Academy of Sciences; Prague, Czech Republic.*

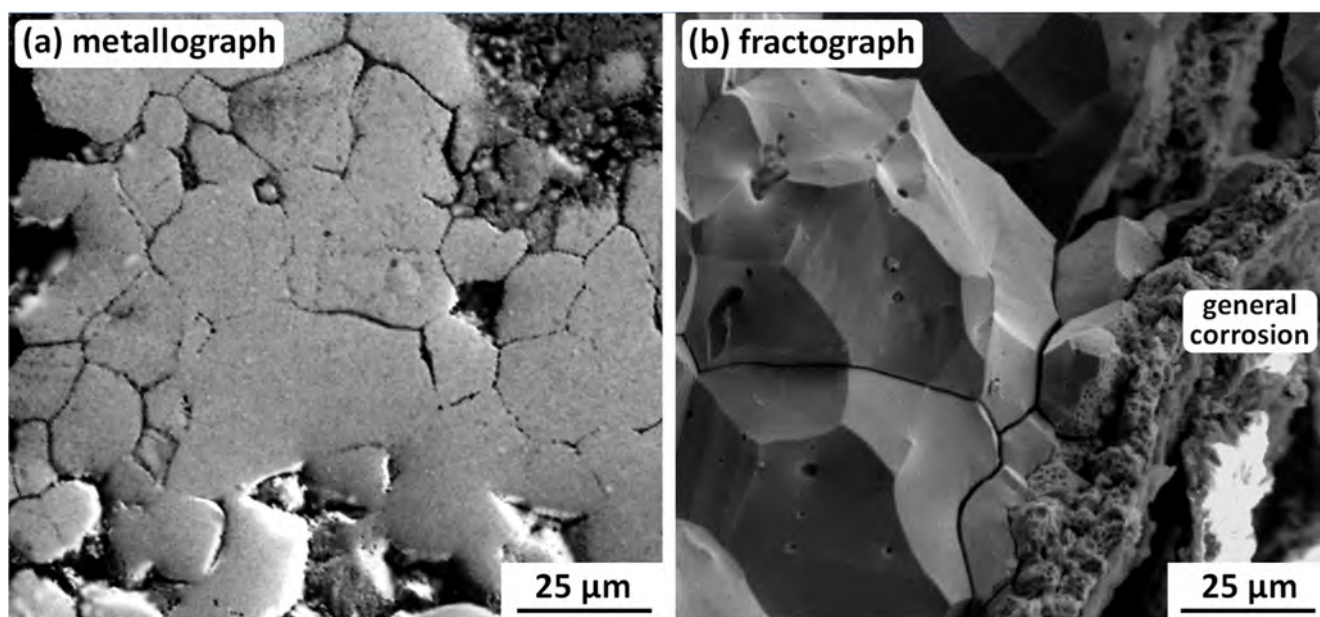


**Figure 11.** Example SEM SE metallograph and fractograph showing (a) corrosion pitting coalescing to form intergranular cracks, and (b) intergranular SCC being destroyed by general corrosion proceeding inwards from a side surface [72]. *Original images with permission: Pavel Bartuška, Institute of Physics, Czech Academy of Sciences; Jaroslava Vaničková, Institute of Chemical Technology; Prague, Czech Republic.*

It is important to note that the fractograph in Figure 11b is from a sample broken open in the laboratory [69], i.e., the intergranular SCC fracture surfaces were close together until then. This means that SCC nucleated and grew with very limited access to the external burial environment, i.e., it occurred under oxygen-depleted conditions that must have prevented general corrosion within the crack. This may be explained with the aid of Figure 12, a silver-water-chloride Pourbaix diagram derived from McNeil and Little [26]:

- Line (a) is the oxygen line above which water is thermodynamically unstable with respect to the generation of oxygen gas.
- Line (b) is the hydrogen line below which water is thermodynamically unstable with respect to the generation of hydrogen gas.
- Between lines (a) and (b), water is thermodynamically stable.
- Line (c) separates stability regions for silver chloride (AgCl) and metallic silver, Ag (metal).
- The upper shaded region represents conditions easily achieved in stagnant waters in a near-surface archaeological environment.
- The lower shaded region indicates other conditions possible in the biosphere.

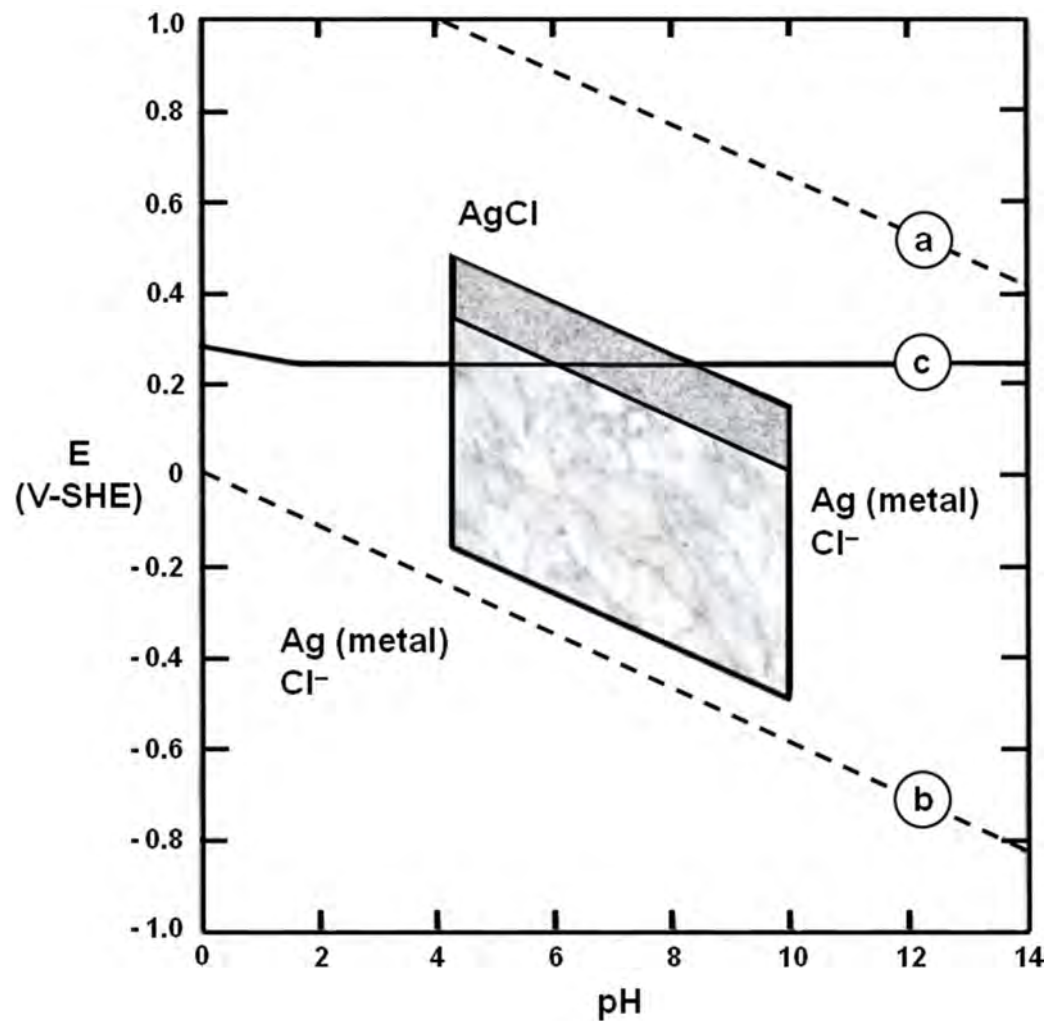


**Figure 12.** Pourbaix diagram for a silver–water–chloride system: After McNeil and Little [26]. The upper shaded region represents conditions readily achieved in stagnant waters in a near-surface archaeological environment. The lower shaded region indicates other conditions possible in the biosphere. For further explanation, see the main text.

If the oxygen content of the water decreases, the conditions that govern corrosion shift downwards on the diagram [26,73]. This makes it increasingly likely that these conditions will fall below line (c). When this occurs, general corrosion ceases but SCC is possible for a wide range of environmental water pH, provided that (i) the metal (a high-silver alloy) is susceptible to SCC, and (ii) tensile stresses are present in the metal. The evidence from the Kaptorga and the other five case histories is consistent with these two conditions [72].

### 3.3.2. Gundestrup Cauldron, 1st–2nd Century BC

The Gundestrup Cauldron and analysis program, using small metallographic samples from different parts of the Cauldron, is shown in Figure 13. The Cauldron was found dismantled in a Danish peat bog in 1891. It has been reversibly assembled and is now in the National Museum of Denmark, Copenhagen. As may be seen from Figure 13, the Cauldron was made from a high-silver alloy (or alloys) and the sample copper contents varied significantly. It was also found from the EBSD investigation that the samples contained varying amounts of retained cold work. Both these unforeseen variations proved to be important for interpreting the analysis results [71,72], and will be discussed after describing some of the EBSD results (Figure 14); the complete results are available from Wanhill et al. [71,74].



**Figure 13.** Gundestrup Cauldron and outline of the investigation: EPMA = Electron Probe Microanalysis; EBSD = Electron Backscatter Diffraction. NLR = Nationaal Lucht- en Ruimtevaartlaboratorium (National Aerospace Laboratory), the Netherlands. *Original image:* Wikipedia.

The EBSD images in Figure 14 are arranged top-down in the order of increasing retained cold work in the samples. Sample 363 is omitted because the results were similar to those of sample 361. The images show the following:

**Sample 366:** Annealed microstructure, shown by solid color equiaxed grains and annealing twins (seen as yellow parallel lines) on the boundary rotation angle map; discontinuous precipitation of copper at grain boundaries (arrows point to examples).

**Sample 361:** Retained cold work shown by (i) color shifts in grains and annealing twins; (ii) dislocations (red) mainly near grain boundaries and deformation twins (narrow-spaced irregular yellow lines) on the boundary rotation angle map. The internal black areas represent intergranular corrosion, which was preferentially associated with retained cold work.

**Sample 365:** Extensive retained cold work shown by (i) elongated grains with more color shifts; (ii) widespread dislocations and numerous deformation twins on the boundary rotation angle map. The internal black areas are mixtures of intergranular and transgranular corrosion, which appears predominant in this sample.

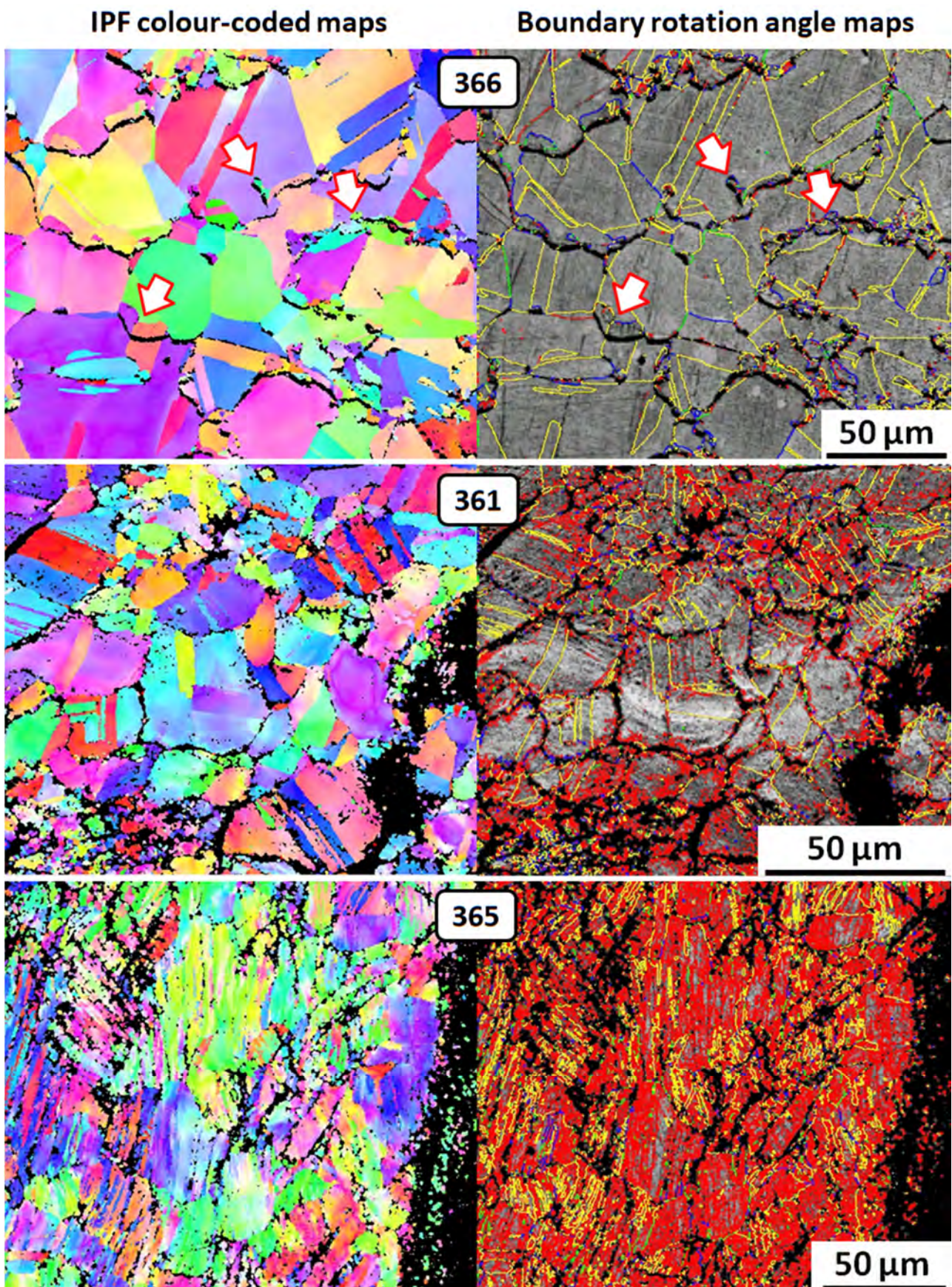
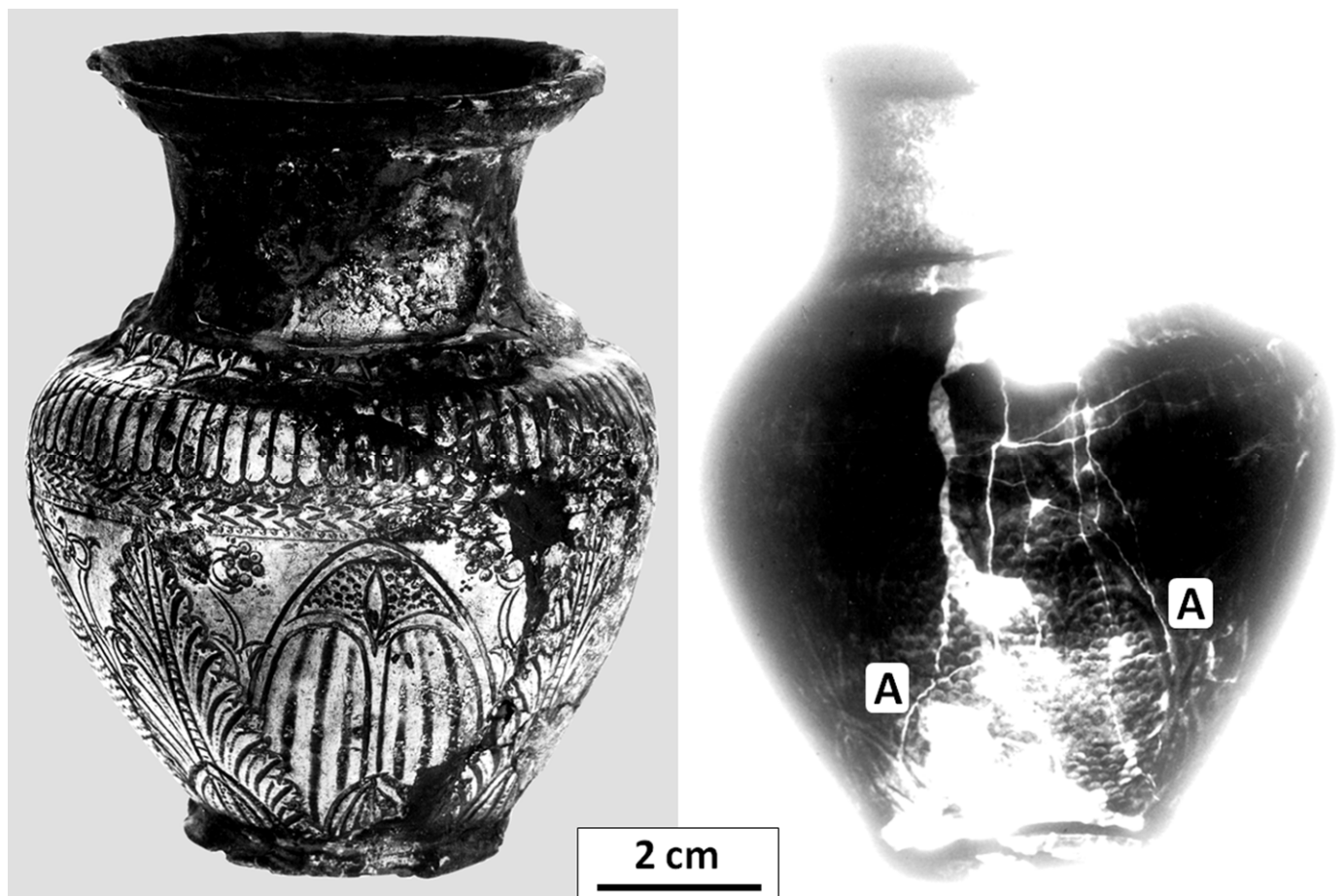


Figure 14. EBSD images for three of the Gundestrup Cauldron samples; discussion in the main text.

These results indicate that retained cold work is primarily responsible for the corrosion damage, and that increasing amounts of retained cold work gradually shift the corrosion damage from intergranular to transgranular. Retained cold work also appears to have suppressed the discontinuous precipitation of copper. For example, the annealed sample, 366, showed extensive precipitation, but sample 361, containing a moderate amount of retained cold work, did not. This difference is emphasized by the fact that sample 361 contained more copper (4.64 wt.%) than sample 366 (3.44 wt.%), as seen in Figure 13 and Wanhill et al. [71,74]. The role of discontinuous precipitation in corrosion-induced embrittlement is discussed in Section 3.5.

### 3.3.3. Egyptian Vase, 2nd–3rd Century BC

The Egyptian Vase is shown in Figure 15. The X-ray radiograph reveals (i) much of the vase is missing and (ii) an ‘egg-shell’ pattern of large cracks. Two of these cracks, labelled [A], follow external chasing grooves. The Vase was restored early in the 20th Century and is fragile owing to a synergistic combination of corrosion-induced embrittlement and microstructurally induced intergranular embrittlement. This latter type of embrittlement is discussed in Section 3.4 for a Roman Kantharos and the Vase.



**Figure 15.** Egyptian Vase photograph and X-ray radiograph showing extensive damage, missing pieces, brittle cracking patterns, and hairline cracks [A] following external decoration (chasing) grooves. *Original images with permission: Ron Leenheer, Allard Pierson Museum; Roel Jansen, University of Amsterdam; the Netherlands.*

The Vase’s average composition, determined by fully quantitative EDX/EDS of three samples, is 97.1 wt.% Ag, 0.9 wt.% Cu, 0.8 wt.% Au, 0.2 wt.% Sn, 0.7 wt.% Pb, and 0.3 wt.% Sb [68]. Significantly, as will be mentioned in Section 3.5, bismuth (Bi) was not detected. Furthermore, the relatively high silver purity and low copper content (in archaeological

terms) means that in the annealed condition, the vase would have been overly liable to deformation during handling. In fact, the Vase samples were found to contain significant amounts of retained cold work [68].

Two samples from the lip and lower wall of the Vase were examined by SEM Back Scattered Electron (BSE) metallography, which revealed more detail than SE imaging and SEM fractography. The microstructures showed the following details [68]:

- Copper-rich segregation bands, which were the remains of coring during the alloy solidification. The bands suggest many cycles of cold working and annealing during fabrication of the Vase. They varied in width from about 2–25  $\mu\text{m}$ . N.B.: Coring occurs even in very dilute silver alloys [75].
- Equiaxed grains 20–200  $\mu\text{m}$  in diameter and occasional annealing twins.
- Local regions of high plastic deformation characterized by slip lines but also by some deformation twins.
- Surface-connected cracks: Mainly wide intergranular cracks, some narrow along slip lines, and twin boundaries. The significance of the crack widths is discussed below.
- Internal cracks: Mainly along segregation bands and only partly intergranular or crystallographic.
- General corrosion on the original external surfaces. Internal corrosion mainly along slip lines but also along twin boundaries and some segregation bands. This corrosion must have been caused by penetration of burial environment moisture along surface-connected slip lines, twin boundaries, and intergranular cracks; and also by access to internal cracks.

Relatively wide intergranular cracks are a pointer to their being caused by microstructurally induced embrittlement, see Section 3.4, rather than corrosion-induced embrittlement. In addition, the presence of significant amounts of retained cold work would likely favor transgranular rather than intergranular corrosion-induced embrittlement, as observed for the Gundestrup Cauldron.

The metallograph in Figure 16 shows some of these microstructural features, especially the segregation bands, localized intense slip, and a 0.1 mm crack growing from the inside surface of the Vase. This metallograph is from the lower wall of the Vase, and has been selected to show the influence of chasing, which is schematically presented next to the metallograph. The schematic shaded deformation pattern is based on more detailed metallographic imaging [68] and slip-line field theory, including the  $t/W$  thickness-to-width ratios [76]; an outline of this pattern is partly discernible in the Figure 16 metallograph. The slip-line field theory predicts a tension zone opposite the indented chasing groove when  $t_i/W = 4.4$ , which is close to the actual value.

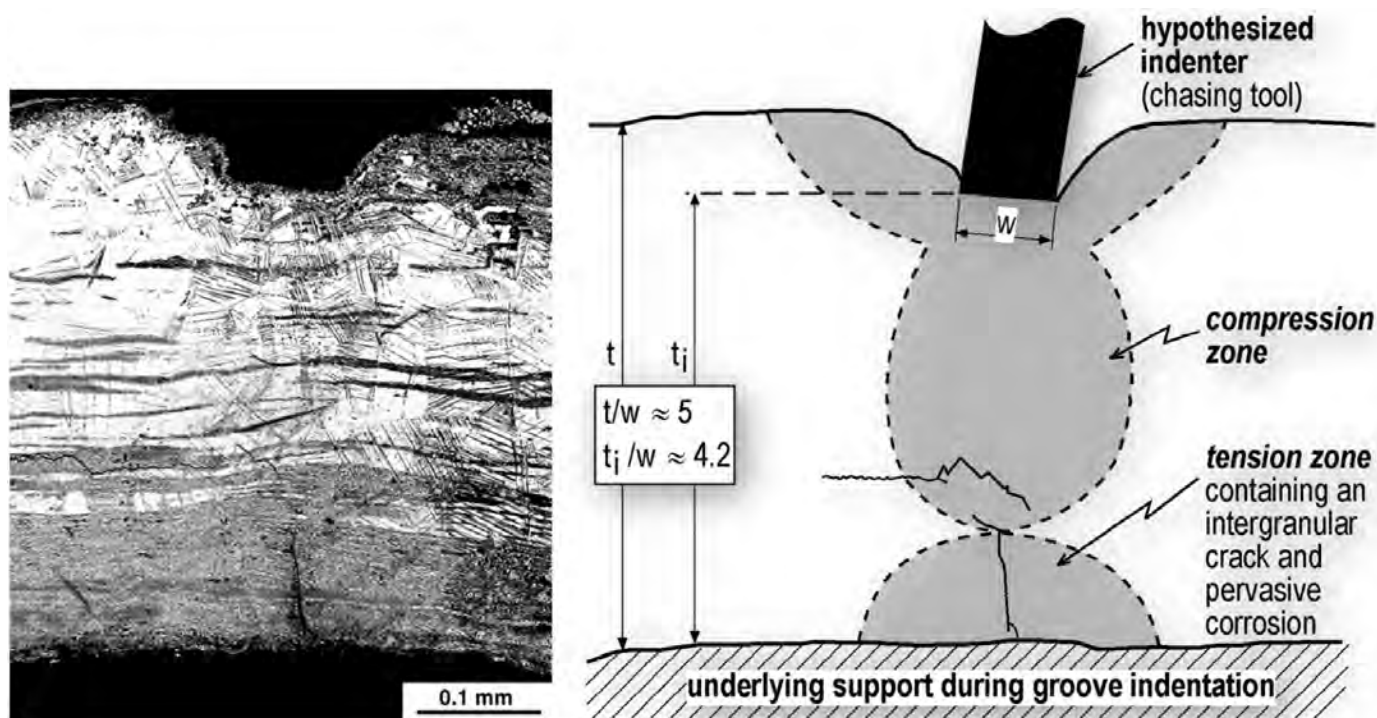


**Figure 16.** SEM BSE metallograph and plasticity theory schematic of the Egyptian Vase lower wall sample containing a chasing groove indent. *Original images:* Russell Wanhill, Emmeloord, The Netherlands [77].

As pointed out previously [78], the evidence in Figure 16 and its interpretation are significant for all high-silver thin-walled artifacts with indented (chased) decorations. If they show evidence of corrosion damage, which is often the case, conservation efforts should include examination for damage and cracking at and near the corresponding internal or rear surface locations.

Owing to the occurrence of synergistic embrittlement in the Vase, whereby much of the intergranular cracking could be due to microstructurally induced embrittlement, the fractographic aspects *definitely* associated with corrosion-induced embrittlement are limited to transgranular cracking, illustrated in Figure 17. The three fractographs show successive stages, beginning with (a) slip line corrosion (pitting at dislocation emergence sites on grain boundaries), then (b) slip plane cracking, and finally (c) crystallographic fracture into blocks. More details are given in Wanhill [72], but here it is important to note that this series of fractographs was possible only because intergranular microstructural embrittlement enabled the fracture of a sample during laboratory investigation.

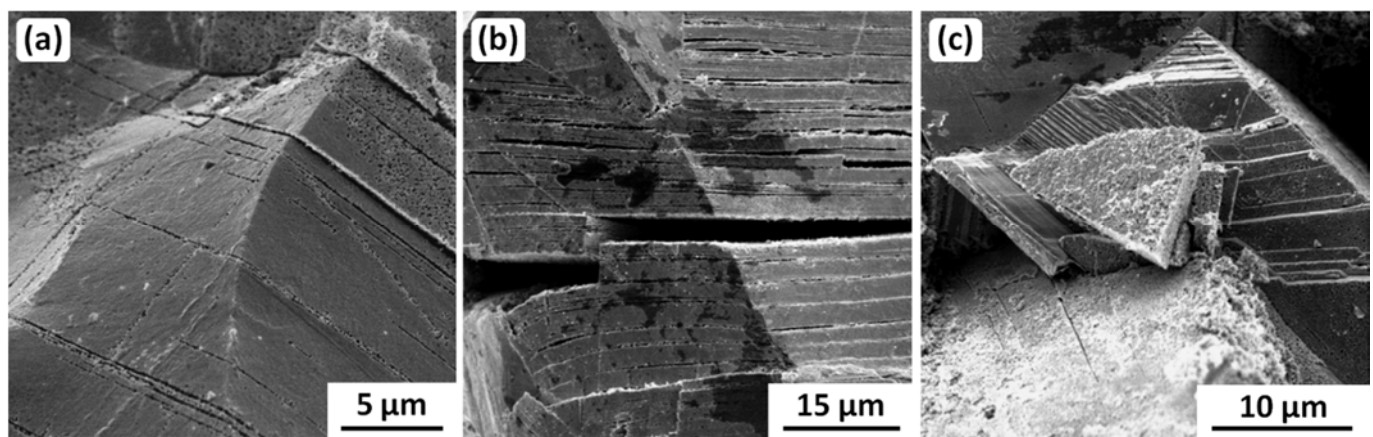


**Figure 17.** Example SEM SE fractographs from the Egyptian Vase samples, showing progressive transgranular SCC: (a) Slip line corrosion (pitting at dislocation emergence sites on grain boundaries), (b) slip plane cracking, and (c) crystallographic fracture into blocks. *Original images with permission: Tim Hattenberg, Netherlands Aerospace Centre, Marknesse, the Netherlands.*

### 3.4. Microstructural Embrittlement

It has long been known that certain elements embrittle silver, specifically antimony [57], lead, and tin [79]. The first metallurgically detailed study is probably due to Thompson and Chatterjee [80]. They studied the age-hardening embrittlement of Ag-Pb and Ag-Pb-Cu alloys, prompted by the brittleness and chemical compositions of ancient silver coins, which would have been ductile when made. They concluded that lead precipitation from the supersaturated solid solution in the silver matrix resulted in embrittlement. However, atomic solute segregation to grain boundaries is most probably sufficient [X16, X30]. Two examples will be discussed in Sections 3.4.1 and 3.4.2, amplified by a concise discussion of microstructural embrittlement in Section 3.5.

#### 3.4.1. Roman Kantharos, 1st Century BC–AD 100

The Roman Kantharos (drinking cup) is shown in Figure 18. It consists of inner and outer cups, with the outer cup riveted to a cast foot. The arrow points to a large crack in the inner cup, which has a bulk composition greater than 97 wt.% Ag. X-ray Fluorescence (XRF) analysis of a (small) sample showed the main other elements to be 0.58–0.63 wt.% Au, 0.45–0.63 wt.% Cu, 0–0.29 wt.% Sn, and 0.16–0.25 wt.% Pb. As in the case of the Egyptian Vase (see Section 3.3.3), bismuth (Bi) was not detected.

Both cups have been severely embrittled by extensive cracking. They were non-reversibly restored by cleaning with acetone, applying an epoxy resin with the intention of filling the cracks, cleaning again, and applying a protective resin to the inner and outer surfaces. However, this treatment failed to properly fill the cracks. Comments on this problem are included in Section 5.3, which discusses the use of coatings in conservation and restoration.



**Figure 18.** Roman Kantharos, inner and outer cups: The arrow points to a large crack in the inner cup. *Original image with permission: Ronny Meijers, Museum Het Valkhof, Nijmegen, The Netherlands.*

A small, recently broken sample from the inner cup was briefly examined in an SEM by the Netherlands Institute for Cultural Heritage (ICN), and the images were made available to the NLR. An example is given in Figure 19. The larger-grained substrate below the planishing layer shows very brittle intergranular fracture with both narrow and wider cracks (arrowed) representing bodily displaced grains. These features are diagnostic for microstructurally induced embrittlement.

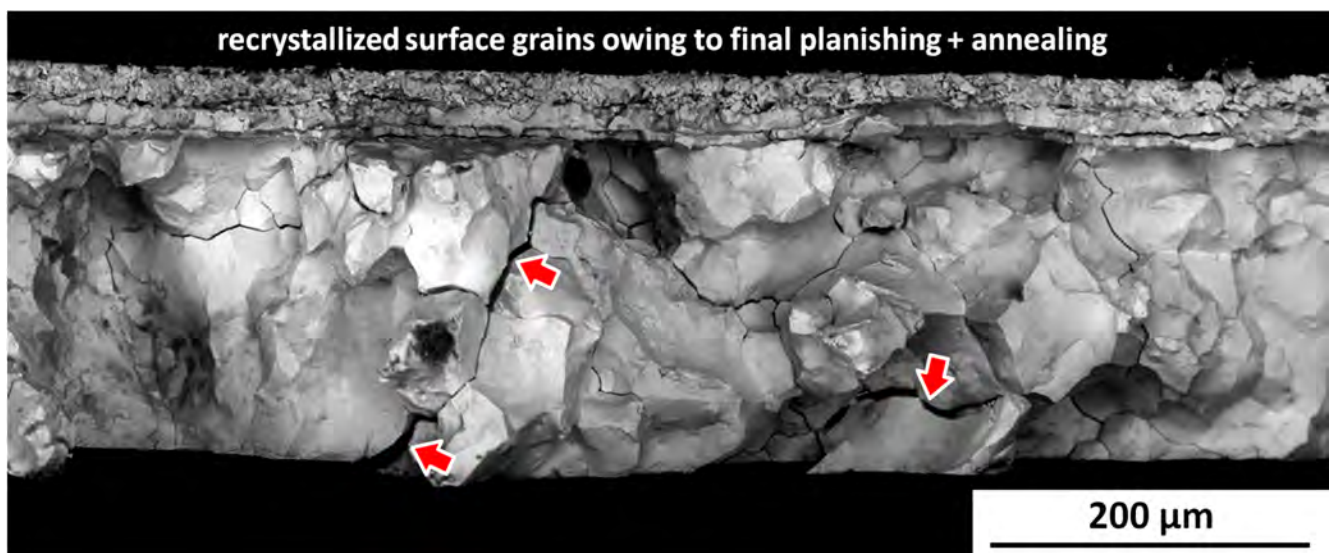


**Figure 19.** Example SEM BSE fractograph for the Kantharos inner cup: Note the brittleness and bodily displaced grains with widened cracks (arrowed). These features are diagnostic for microstructural embrittlement. The black ‘smudges’ are non-metallic contamination. *Original image with permission: Ineke Joosten, Netherlands Institute for Cultural Heritage (ICN), Amsterdam, The Netherlands.*

### 3.4.2. Egyptian Vase, 2nd–3rd Century BC

The Egyptian Vase, an overview of the types of damage to it, its chemical composition, and corrosion-induced embrittlement have been described and discussed in Section 3.3.3. Here, an example of microstructural embrittlement is presented. Figure 20 gives an example distinguishing microstructurally induced embrittlement from transgranular corrosion-

induced embrittlement, which is represented by slip line attack and transgranular blocks of slip plane cracking.



**Figure 20.** Example SEM SE fractograph for the Egyptian Vase showing (i) bodily displaced grains and consequently widened cracks diagnostic for microstructural embrittlement, (ii) slip line attack and transgranular blocks of slip plane cracking diagnostic for SCC of cold-worked high-silver artifacts. *Original image with permission:* Tim Hattenberg, Netherlands Aerospace Centre, Marknesse, the Netherlands.

### 3.5. The Role(s) of Discontinuous Precipitation of Copper

Over more than four decades (1965–2012), there have been several suggestions about the significance of discontinuous precipitation of copper at the grain boundaries of ancient silver [66,67,69,70,81–83]. A review comprising seven case histories (including the Kaptorga, Cauldron, Vase, and Kantharos in the present paper), additional information on discontinuous precipitation, and empirical and theoretical metallurgical considerations [84] was published in 2012 [85]. A summary is given here:

*Copper precipitation and embrittlement:* The significance of discontinuous precipitation of copper for the embrittlement of ancient silver is limited. Discontinuous precipitation may facilitate the process of intergranular corrosion-induced embrittlement, but is not the primary cause. Nor is it responsible for transgranular corrosion-induced embrittlement and microstructurally induced embrittlement, which is most probably due to atomic solute segregation of lead to grain boundaries. A possible alternative to lead is bismuth [81], but it is noteworthy that while lead was present in the Vase and Kantharos, bismuth was not detected. This means that if bismuth were present, it would be in much smaller amounts than lead, and therefore less likely to cause or even contribute to embrittlement.

*Copper precipitation and authenticity:* It has been proposed that the precipitate widths and its detailed morphology could be used to date and hence authenticate ancient silver objects [83,84]. The dating possibility is invalid, as demonstrated by metallography of the annealed sample 366 from the Cauldron and the extrapolated Arrhenius-type reaction kinetics of copper precipitation at ambient temperatures [85]. However, in combination with information on provenance and stylistic aspects, the presence of discontinuous precipitation in a silver object may be regarded as additional evidence of antiquity.

#### 4. Diagnostic Techniques and Analysis Methods

The previous sections on corrosion and embrittlement of ancient copper and high-silver alloys have mentioned a number of analytical techniques and methods. In this section, we provide an overview of the context and usefulness of these techniques and methods. Table 6 surveys the most relevant diagnostic techniques used in answering questions that are, or may be, posed by ancient metallic objects. The scientific methods are mainly complementary, but there is some overlap that enables broader and more definitive views. This is particularly relevant to damage assessments of broken or severely cracked and embrittled objects, since in our experience, fractographic damage assessments are seldom done, yet the results can be important for conservation and restoration.

**Table 6.** Archaeological and archaeometallurgical questions and diagnostic techniques.

Archaeological and Archaeometallurgical Questions	Diagnostic Techniques
<ul style="list-style-type: none"> <li>● Basic identification and provenance</li> </ul>	<ul style="list-style-type: none"> <li>● Classical archaeology</li> </ul>
<ul style="list-style-type: none"> <li>● Further identification and provenance               <ul style="list-style-type: none"> <li>○ metal and alloy compositions</li> <li>○ origins of metals and ores</li> <li>○ authenticity: genuine, modern and ancient fakes</li> </ul> </li> </ul>	<ul style="list-style-type: none"> <li>● Isotopes and chemical analyses, various methods available; some metallography</li> </ul>
<ul style="list-style-type: none"> <li>● Manufacturing and craftsmanship               <ul style="list-style-type: none"> <li>○ mechanically worked, mechanically worked and annealed, grain size, segregation bands, slip lines, annealing and deformation twins</li> <li>○ as-cast, cast and annealed, dendrite coring, dendrite and grain sizes, eutectic sizes and distributions</li> <li>○ alloy phases, matrix and grain boundary precipitates, constituent particles, inclusions, porosity</li> </ul> </li> </ul>	<ul style="list-style-type: none"> <li>● The features in this topic, <i>and also most corrosion damage</i>, are investigated mainly by metallography, in combination with various chemical analysis methods</li> </ul>
<ul style="list-style-type: none"> <li>● Damage assessment               <ul style="list-style-type: none"> <li>○ deformation, formation of internal voids during tensile elongation and ductile fracture</li> <li>○ surficial and internal corrosion; corrosion layers</li> <li>○ embrittlement, cracks and fractures: microstructurally induced; corrosion-induced, especially SCC</li> </ul> </li> </ul>	<ul style="list-style-type: none"> <li>● <b>Macro:</b> visual inspection, including use of stereo binoculars; X-ray radiography <b>Micro:</b> mainly fractography except <i>most corrosion damage</i>, where corrosion layers and products are better examined by metallography and chemical analysis</li> </ul>

##### 4.1. Further Identification and Provenance

Metallurgically based contributions to further identification and provenance fall into two categories, isotope analysis and chemical analysis:

*Isotope analysis:* The greatest use of this method has been the determination of lead isotope ratios in ore deposits, mines, slag heaps, and ancient metal objects. This activity was initiated in the 1970s, and has been extensively reviewed by two long-term experts [86]. Initially, the focus was on bronze age lead and silver, e.g., [59,87]. However, the method was soon extended to copper alloys [88]. Since these early results, there has been considerable debate about lead isotope analysis, but improvements in the methodology over the last decades have made it more reliable [89]. More recently, a project to determine whether the provenance of ancient bronzes might be obtained from copper and tin isotope analyses has shown some promise [90]. Notwithstanding these developments, provenance

determination from isotope analyses remains a complex and challenging diagnostic technique [91], but the results can have major implications for understanding the use, recycling, and circulation of metals in ancient times [92].

*Chemical element analysis:* ICP-OES and ICP-MS are suitable for accurate and precise multi-element measurements down to trace element levels (ppm range) for metals, alloys, and corrosion products, requiring only small solid samples (0.5–2 g). Disadvantages are the high costs of the equipment and hence the availability. Less-discriminating bulk analyses are commonly done with small SEM samples, using EDX/EDS (energy-dispersive) or WDX/WDS (wavelength-dispersive) equipment, preferably calibrated with standards for optimum accuracy and precision. In practice, EDX/EDS is most commonly used, yet another possibility is EPMA. This is fundamentally the same as using an SEM with EDX/EDS or WDX/WDS, but EPMA is specialized for higher-accuracy quantitative analysis rather than sample imaging. However, the general availability of EPMA equipment is much less than that of SEMs. Finally, a very useful ‘in-the-field’ semi-quantitative and non-destructive method is provided by portable (handheld) XRF equipment, including portable micro-XRF.

#### 4.2. Manufacturing and Craftsmanship

*Metallography:* As Table 6 shows, metallography is a versatile and powerful technique for investigating metallic archaeological objects. Optical metallography is very useful up to about X1500 magnification, especially for the examination of etched samples. Careful selection of polishing and etching procedures can reveal much about the microstructures [93]. The capabilities of metallography have been greatly extended by the advent of commercial SEMs in the mid-to-late 1960s. These cover the range of X10–X20,000 for conventional SEMs, and up to about X40,000 for field-emission gun microscopes (FE-SEMs). Moreover, SEMs can be used with EDX/EDS and WDX/WDS equipment to provide local chemical analyses of the bulk metal, alloy phases, segregation bands, precipitates, and inclusions, as can be seen above. Another important capability added to SEMs is EBSD, e.g., see the Gundestrup Cauldron sample images in Figure 14. These are some of the first, if not the first, EBSD images to be published for an ancient metallic artifact [74]. A guide to metallographic preparation for EBSD analysis has also been published [94,95].

#### 4.3. Damage Assessment

*Visual and X-ray inspections:* Visual inspection with unaided eyes, a hand lens (X1–X10), and a stereobinocular (X10  $\approx$  X50), with (color) photographs taken as required. The purpose is to assess the object’s basic condition (nominally intact or restored; any missing pieces and large cracks). X-ray inspection is complementary to visual inspection and also enables detecting ‘hidden damage’, e.g., internal cracks, as seen in the Egyptian vase in Figure 15. Access to traditional X-ray equipment can be a problem, let alone access to a computerized tomography (CT) scanner, should that be considered advantageous or even necessary.

*Metallography:* Optical and SEM metallography are well-suited to assessing the extent and types of corrosion damage, especially when SEMs are used with EDX/EDS and WDX/WDS to detect the elements present in the corrosion layers.

*Chemical phase analysis:* XRD is useful for analysis of the chemical nature of corrosion products, e.g., as described by Oudbashi et al. [40].

*Fractography:* Fracture surface analysis is a minor or non-existent consideration for most archaeometallurgical studies [52]. However, it is a useful adjunct to metallography, notably for damage assessment. This is because detailed fractography can improve restoration and conservation procedures by identifying the extent and sources of damage. Visual inspection, including macrophotographs, should be done before proceeding to SEM fractography. Furthermore, it can be most helpful to break open embrittled samples to reveal details unobscured by long-term corrosion products; examples are given in Figure 9, Figure 11b, and Figure 17. Sometimes, it is possible to combine SEM fractography with EDS/EDX analysis of fracture surface details, e.g., segregation bands and inclusions, although accuracy will

often be limited owing to the lack of smooth and ideally orientated surfaces with respect to the primary electron beam.

## 5. Restoration and Conservation of Corroded and Embrittled Artifacts

Restorations have ethical and technical issues. Any restoration should (i) respect an artifact's integrity, meaning veracity rather than wholeness, and (ii) be reversible. However, the second meaning, wholeness, can override reversibility when needing to preserve severely embrittled and fragmented high-value artifacts [64,96–99]. For example, the Kaptorga, Egyptian Vase, and Kantharos have all been non-reversibly restored, while the Gundestrup Cauldron could be disassembled, however unlikely the need for it. There are several Handbooks available for different classes of metals and alloys, e.g., [4,23,64,100], but detailed technical guidelines differ, depending on a particular artifact's condition. Some comments follow, using this paper's case studies where possible, and also including the famous Khan Cup [99]. A final section briefly reviews conservation coatings, and their advantages and disadvantages.

### 5.1. Bronzes and Other Copper-Based Alloys

Corrosion is the major problem in the conservation of ancient bronzes and other copper-based alloys. Corrosion can be responsible for fragility, breakage, and even complete destruction of an artifact, e.g., [46]. A large variety of corrosion products have been found on ancient copper alloys [24,46,101], some of which are harmful, but others result in attractive patinas that need preservation. A particularly damaging type of corrosion is 'Bronze Disease' [22–24,102]. Selwyn and Hamilton [22,23,102] describe this type of corrosion in detail and how to treat it, as well as less damaging corrosion:

*Initial cleaning:* Patina preservation by extended washing in water or a sodium sesquicarbonate solution; careful mechanical cleaning and rinsing in water; or immersing in e.g., a citric acid solution inhibited with thiourea until encrustations are removed. There are other possible chemical solutions [22,23,102].

*Bronze Disease:* Applicable when artifacts are contaminated by chlorides. The treatments may be chemical or electrochemical. However, care is needed in the choice of chemicals and in using electrochemical techniques, which may be too aggressive if the corrosion layers are thin. The currently favored method(s) are treatment with an ethanol solution of benzotriazole (BTA), either in an ambient air environment or under vacuum, followed by drying with acetone or a water-miscible alcohol.

*Repairs:* These may be desired for display purposes. Acrylic-containing adhesives are favored, since they are removable, like acrylic coatings [23].

*Coatings:* Use a clear acrylic lacquer or microcrystalline wax. Suitable lacquers are Paraloid B72 or Acryloid B48. These are removable if and when required; also see the Khan Cup restoration described in the next subsection on high-silver alloys.

In addition, it is necessary to plan for long-term conservation and provide the required equipment and procedures [103]: (i) Establish a recording system for the relative humidity (R.H.) in storage room and museum environments; (ii) install portable dehumidifier equipment in the storage room to keep the R.H. lower than 50%, preferably 42–46%, over a wide range of ambient temperatures., thereby preventing active corrosion, notably Bronze Disease, from reoccurring [24,104]; (iii) use desiccants, e.g., silica gel, in display cases, since display rooms do not usually have controlled environment systems; and (iv) institute a periodic monitoring system.

### 5.2. High-Silver Alloys

Restoration and conservation of high-silver embrittled artifacts present a number of issues: (i) They can be very fragile, as illustrated by the Kaptorga, Egyptian Vase, and Kantharos case studies; (ii) it is important, or should be important, to determine the cause(s) of embrittlement in order to select the best treatments; (iii) coatings should be considered for long-term conservation; and (iv) despite a variety of options, the best or only feasible

treatments may be non-reversible. As mentioned at the beginning of this main section, the treatments for all three case studies are non-reversible.

An outstanding example of the aesthetic benefits of restoration, making some treatment stages reversible, is the Khan Cup [99], dated to the AD 13th Century. Figure 21 shows the Cup before and after restoration.

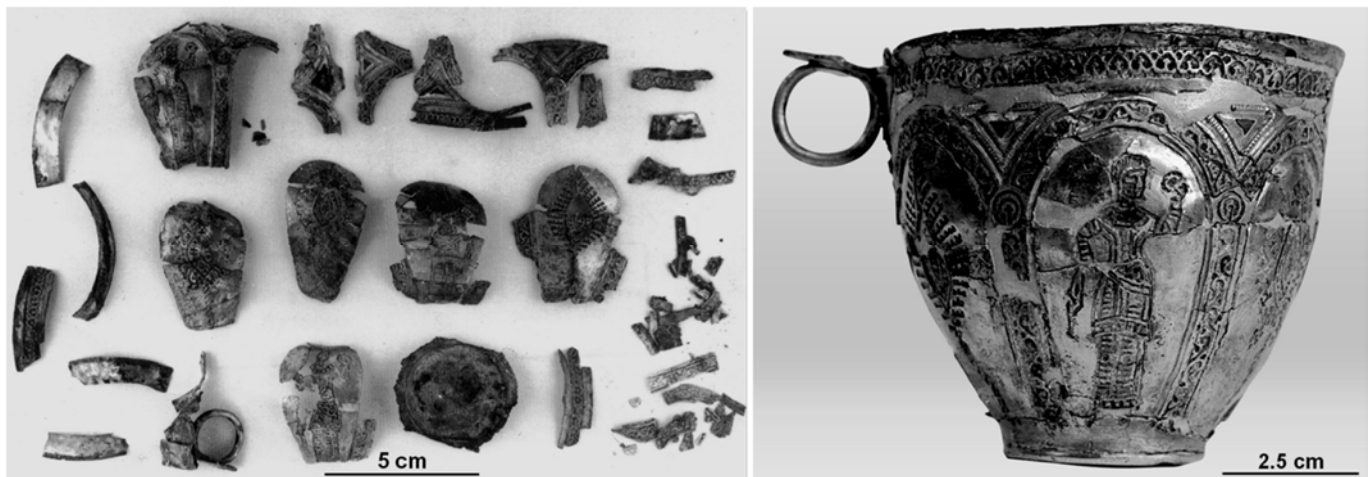


**Figure 21.** Khan Cup before and after restoration. *Original images with permission:* Gerhard Stawinoga, Archäologisches Landesmuseum, Schleswig, Germany.

Besides enabling the Cup to be aesthetically appreciated, the restoration showed how it had been fabricated, and the final step included a removable protective coating. In more detail, the restoration sequence was as follows [99]:

- Previously crudely glued fragments (154 in total) were disassembled, the corrosion removed by silver polish, rinsed in distilled water, and dried in acetone.
- Strongly deformed fragments were supported by a rubber backing and partially or wholly reshaped by applying light pressure with burnishing tools (steel or hard wood).
- External fixation: Partial assembly by fixing fragments with strips of adhesive tape; full assembly required joining under stress using wooden clamps and fixation with glass silk impregnated by Mecosan (an adhesive removable with acetone).
- Internal joining during partial and full assembly using glass silk and Mecosan or a cyanoacrylate (Super Glue).
- After full assembly, the external fixation was removed using acetone.
- Exposed internal glass silk (covering gaps in the full assembly) was pigmented using silver powder mixed with Paraloid B72, a clear non-yellowing lacquer and removable with acetone and toluene.
- Final coating of the restored Cup with Paraloid B72 dissolved in toluene.

Obviously, the fragment reshaping operation is (was) non-reversible. It was also (unintentionally) diagnostic. Although the fragments were not studied in detail, the fact that they could be reshaped without further fragmentation suggests that embrittlement was not intrinsic (microstructurally induced); i.e., the cause of cracking and fracture was most probably SCC.

An important point relevant to the Khan Cup and mentioned in Section 3.3.3 with respect to the Egyptian Vase is the likely presence of residual stresses induced by indented (chased) decorations. These stresses, tensile on the internal or rear sides of thin-walled artifacts, have been implicated in the occurrence of SCC in ancient silver [72]. Thus, conservation efforts should include examination for decoration-induced damage and cracking at the corresponding internal or rear side locations. If such damage is detected, then the final restoration (or conservation) step should include coating on both sides.

### 5.3. Coatings for Preservation and Conservation

The choice of coatings for the conservation of ancient and historic metallic objects is important. Much information is available [23,102,105–107], and Table 7 summarizes the requirements, types of well-established coatings, and their advantages and disadvantages. Microcrystalline waxes and acrylics are often used [22,23,102,105,106]. For example, two layers of microcrystalline wax were applied to the Egyptian Vase after surface cleaning, and the Paraloid B72 coating for the Khan Cup is acrylic-based.

**Table 7.** Survey of well-established conservation and preservation coatings.

<ul style="list-style-type: none"> <li>● <b>Coating requirements</b> <ul style="list-style-type: none"> <li>○ ambient temperature application: preferable or essential</li> <li>○ colorless and transparent: no age-yellowing, long-term stability</li> <li>○ <i>ideally</i> conformal (uniform closely controlled thickness and pin-hole free)</li> <li>○ low permeability to moisture and corrosive gases (e.g. atmospheric H<sub>2</sub>S)</li> <li>○ high crevice and crack penetration (<i>ideally</i>)</li> <li>○ removable, i.e. <i>reversible</i>: preferable or essential</li> </ul> </li> </ul>			
<ul style="list-style-type: none"> <li>● <b>Coating types</b> <ul style="list-style-type: none"> <li>○ acrylics</li> <li>○ cellulose nitrate</li> <li>○ wax</li> </ul> </li> </ul>	<ul style="list-style-type: none"> <li>● <b>Application</b> <ul style="list-style-type: none"> <li>○ liquid except wax</li> <li>○ normal air</li> </ul> </li> </ul>	<ul style="list-style-type: none"> <li>● <b>Advantages</b> <ul style="list-style-type: none"> <li>○ removable but probably not feasible for severely embrittled objects</li> <li>○ controllable thickness</li> <li>○ pinhole-free</li> <li>○ crevice/crack penetration</li> <li>○ most moisture removed</li> </ul> </li> </ul>	<ul style="list-style-type: none"> <li>● <b>Disadvantages</b> <ul style="list-style-type: none"> <li>○ thickness variations</li> <li>○ possible pinholes</li> <li>○ poor crack penetration</li> <li>○ entrapped moisture</li> </ul> </li> </ul>
<ul style="list-style-type: none"> <li>○ parylenes</li> </ul>	<ul style="list-style-type: none"> <li>○ vapor phase</li> <li>○ reduced pressure</li> </ul>		<ul style="list-style-type: none"> <li>○ not removable below 150 °C</li> <li>○ special equipment</li> </ul>

Table 7 also includes parylenes. These have been used to preserve books, fragile biological objects, and a 19th Century brass microscope [108], but seem not to have been used for ancient metallic objects. There are two significant disadvantages in using parylenes: (i) They cannot be removed at ambient temperatures and (ii) their application requires special equipment [109]. On the other hand, a parylene coating could be considered for crack-filling and consequent mechanical stabilization of high-value severely embrittled artifacts. This suggestion is motivated by additional fractographic evidence from the Kantharos case study: As mentioned in Section 3.4.1, an epoxy resin failed to properly fill the cracks [52].

Coatings research is continuing [110–114]. Some investigations have compared newer coatings with well-established ones like Paraloid B72. The results show that several types of coatings are suitable for preservation and conservation. These include Poligen, Inralac (a mixture of acrylic polymer and a corrosion inhibitor), carboxylates, nanostructured films, and eco-friendly and non-hazardous coatings based on silanes and fluoropolymers.

## 6. Summary

The relation between corrosion and embrittlement of ancient copper-based and high-silver alloys is complex. General corrosion gradually damages and can eventually destroy artifacts and coins. This has led to specialist restoration and conservation techniques that are widely used. Less well-known and appreciated is the embrittlement threat posed by selective corrosion, namely stress corrosion cracking (SCC), and also microstructurally induced embrittlement in high-silver alloys that can act synergistically with SCC, though this combination appears to be rare [77].

SCC in ancient copper-based and high-silver alloy objects has only recently been recognized as distinct from general corrosion [52,72], and is the main topic of the examples

reviewed in this paper. These examples, and others [77,115], show that combinations of metallography and fractography, which are not usually employed to investigate cracks and fractures in ancient objects, provide useful contributions and insights for damage assessment. Notable examples are the SCC-promoting influences of (i) residual stresses from retained cold work and external chising, and (ii) burial-induced stresses on thin-walled hollow artifacts. In addition, the observation of damage consistent with SCC emphasizes the significance of the burial environment. Burials in graves result in high local salinity [115] and this promotes SCC in many classes of alloys. This is in addition to its role in promoting general corrosion.

It should therefore be no surprise that objects from grave burials can be severely embrittled and must be handled and treated with great care. Examples in the present paper are the bronze vessels from Luristan (Western Iran), and the Kaptorga, Egyptian Vase, and Khan Cup. N.B.: The Kantharos must also be handled with great care, but this is because of microstructurally induced embrittlement, which appears to be much less common [77].

**Author Contributions:** Conceptualization, O.O. and R.W.; writing—original draft preparation, O.O. and R.W.; writing—review and editing, O.O. and R.W. Both authors have read and agreed to the published version of the manuscript.

**Funding:** This research received no external funding.

**Data Availability Statement:** The data presented in this study are available from the corresponding authors.

**Acknowledgments:** We thank the many colleagues who provided information and assistance: Pavel Bartuška, Co Dalemans, Jiří Děd, Ata Hasanpour, Tim Hattenberg, Roel Jansen, Ineke Joosten, Ron Leenheer, Ronny Meijers, Reza Naseri, Afroz Shahinfar, Atefeh Shekofteh, Gerhard Stawinoga, Jarka Vaníčková, Museum het Valkhof, National Museum of Iran, Falak-ol-Aflak Museum of Khorramabad, Royal Netherlands Aerospace Centre.

**Conflicts of Interest:** The authors declare no conflict of interest.

## References

1. Smith, C.S. *A History of Metallography: The Development of Ideas on the Structure of Metals before 1890*; University of Chicago Press: Chicago, IL, USA, 1960.
2. Three thousand years of copper alloys: From the Bronze Age to the Industrial Revolution. In *Application of Science in Examination of Works of Art*; Young, W.J. (Ed.) Boston Museum of Fine Arts: Boston, MA, USA, 1965; pp. 59–67.
3. Scott, D.A. *Metallography and Microstructure of Ancient and Historic Metals*; The Getty Conservation Institute, The J. Paul Getty Trust in Association with Archetype Books: Los Angeles, CA, USA, 1991.
4. Scott, D.A.; Podany, J.; Considine, B.B. (Eds.) *Ancient & Historic Metals, Conservation and Scientific Research*; The J. Paul Getty Museum and the Getty Conservation Institute, The J. Paul Getty Trust: Los Angeles, CA, USA, 1994.
5. Scott, D.A.; Meyers, P. (Eds.) *Archaeometry of Pre-Columbian Sites and Artifacts*; The Getty Conservation Institute, The J. Paul Getty Trust: Los Angeles, CA, USA, 1994.
6. Bailey, J.; Crossley, D.; Ponting, M. *Metals and Metalworking: A Research Framework for Archaeometallurgy*; Occasional Publication No.6; The Historical Metallurgy Society Ltd.: London, UK, 2008.
7. *Archaeometallurgy: Guidelines for Best Practice*; Historic England: Swindon, UK, 2015.
8. Roberts, B.W.; Thornton, C.P.; Pigott, V.C. Development of metallurgy in Eurasia. *Antiquity* **2009**, *83*, 1012–1022. [[CrossRef](#)]
9. Killick, D. From ores to metals. In *Archaeometallurgy in Global Perspective-Methods and Syntheses*; Roberts, B.W., Thornton, C.P., Eds.; Springer: New York, NY, USA, 2014; pp. 11–45.
10. Thornton, C.P. The emergence of complex metallurgy on the Iranian Plateau: Escaping the Levantine paradigm. *J. World Prehist.* **2009**, *22*, 301–327. [[CrossRef](#)]
11. Radivojević, M.; Rehren, T.; Pernicka, E.; Šljivar, D.; Brauns, M.; Borić, D. On the origins of extractive metallurgy: New evidence from Europe. *J. Archaeol. Sci.* **2010**, *37*, 2775–2787. [[CrossRef](#)]
12. Lechtman, H.; Klein, S. The production of copper-arsenic alloys (arsenic bronze) by cosmelting: Modern experiment, ancient practice. *J. Archaeol. Sci.* **1999**, *26*, 497–526. [[CrossRef](#)]
13. Rehren, T.; Boscher, L.; Pernicka, E. Large scale smelting of speiss and arsenical copper at Early Bronze Age Arisman, Iran. *J. Archaeol. Sci.* **2012**, *39*, 1717–1727. [[CrossRef](#)]
14. Müller, R.; Rehren, T.; Rovira, S. Almizaraque and the early copper metallurgy of southeast Spain: New data. *Madr. Mitt.* **2004**, *45*, 33–56.
15. Tylecote, R.F. *A History of Metallurgy*, 2nd ed.; Maney Publishing: London, UK, 2002.

16. Erb-Satullo, N.L.; Gilmour, B.J.J.; Khakhutaishvili, N. Crucible technologies in the Late Bronze Early Iron Age South Caucasus: Copper processing, tin bronze production, and the possibility of local tin ores. *J. Archaeol. Sci.* **2015**, *61*, 260–276. [[CrossRef](#)]
17. Oudbashi, O.; Hasanpour, A. Bronze alloy production during the Iron Age of Luristan: A multianalytical study on recently discovered bronze objects. *Archaeol. Anthropol. Sci.* **2018**, *10*, 1443–1458. [[CrossRef](#)]
18. Merkel, S.W. Calamine of the Bergamasque Alps as a possible source of zinc for Roman brass: Theoretical considerations and preliminary results. *Period. Mineral.* **2021**, *90*, 27–39.
19. Chase, W.T. Chinese bronzes: Casting, finishing, patination and corrosion. In *Ancient and Historic Metals: Conservation and Scientific Research*; Scott, D.A., Podany, J., Considine, B.B., Eds.; Getty Conservation Institute: Los Angeles, CA, USA, 1994; pp. 85–118.
20. Angelini, E.; Rosalbino, F.; Grassini, S.; Ingo, G.M.; De Caro, T. Simulation of corrosion processes of buried archaeological bronze artefacts. In *Corrosion of Metallic Heritage Artefacts: Investigation, Conservation and Prediction for Long-Term Behaviour*; Dillmann, P., Béranger, G., Piccardo, P., Matthiesen, H., Eds.; European Federation of Corrosion Publication 48; Woodhead Publishing: Cambridge, UK, 2007; pp. 203–218.
21. Scott, D.A. *Copper and Bronze in Art: Corrosion, Colorants and Conservation*; Getty Conservation Institute: Los Angeles, CA, USA, 2002.
22. Selwyn, L.S. Corrosion of metal artifacts in buried environments. In *ASM Handbook, Volume 13C, Corrosion: Environments and Industries*; ASM International: Materials Park, OH, USA, 2006; pp. 306–322.
23. Selwyn LS: *Metals and Corrosion: A Handbook for the Conservation Professional*; Canadian Conservation Institute: Ottawa, ON, Canada, 2004.
24. Scott, D.A. Bronze disease, a review of some chemical problems and the role of relative humidity. *J. Am. Inst. Conserv.* **1990**, *29*, 193–206. [[CrossRef](#)]
25. North, N.A.; MacLeod, I.D. Corrosion of metals. In *Conservation of Marine Archaeological Objects*; Pearson, C., Ed.; Butterworths: London, UK, 1987; pp. 63–98.
26. McNeil, M.B.; Little, B.J. Corrosion mechanisms for copper and silver objects in near-surface environments. *J. Am. Inst. Conserv.* **1992**, *31*, 355–366. [[CrossRef](#)]
27. Ingo, G.M.; Riccucci, C.; Guida, G.; Pascucci, M.; Giuliani, C.; Messina, E.; Fierro, G.; Di Carlo, G. Micro-chemical investigation of corrosion products naturally grown on archaeological Cu-based artefacts retrieved from the Mediterranean sea. *Appl. Surf. Sci.* **2019**, *470*, 695–706. [[CrossRef](#)]
28. Selwyn, L.S.; Roberge, P.R. Corrosion of metal artifacts displayed in outdoor environments. In *ASM Handbook Volume 13C, Corrosion: Environments and Industries*; ASM International: Materials Park, OH, USA, 2006; pp. 289–305.
29. Constantinides, I.; Adriaens, A.; Adams, F. Surface characterization of artificial corrosion layers on copper alloy reference materials. *Appl. Surf. Sci.* **2002**, *189*, 90–101. [[CrossRef](#)]
30. Meeks, N. Surface characterization of tinned bronze, high-tin bronze, tinned iron and arsenical bronze. In *Metal Plating and Patination: Cultural, Technical and Historical Developments*; Butterworth-Heinemann Ltd.: Oxford, UK, 1993; pp. 247–275.
31. Mödlinger, M.; Sabatini, B. A Re-evaluation of inverse segregation in prehistoric As-Cu objects. *J. Archaeol. Sci.* **2016**, *74*, 60–74. [[CrossRef](#)]
32. Cerrato, R.; Casal, A.; Mateo, M.P.; Nicolas, G. Dealloying evidence on corroded brass by laser-induced breakdown spectroscopy mapping and depth profiling measurements. *Spectrochim. Acta A* **2017**, *130*, 1–6. [[CrossRef](#)]
33. Fernandes, R.; van Os, B.J.H.; Huisman, H.D.J. The use of hand-held XRF for investigating the composition and corrosion of Roman copper-alloyed artefacts. *Herit. Sci.* **2013**, *1*, 30. [[CrossRef](#)]
34. Ahmed, Z. *Principles of Corrosion Engineering and Corrosion Control*; Elsevier: Amsterdam, The Netherlands, 2006.
35. Weisser, T.S. The de-alloying of copper alloys. *Stud. Conserv.* **1975**, *20*, 207–214. [[CrossRef](#)]
36. Barrena, M.I.; Gómez de Salazar, J.M.; Soria, A. Corrosion of brass archaeological blinker: Characterisation of natural degradation process. *Mater. Lett.* **2008**, *62*, 3944–3946. [[CrossRef](#)]
37. Martens, W.; Frost, R.; Williams, P. Raman and infrared spectroscopic study of the basic copper chloride minerals—Implications for the study of the copper and brass vorrosion and bronze disease. *Neues Jahrb. Miner. Abh.* **2003**, *178*, 197–215. [[CrossRef](#)]
38. Robbiola, L.; Blengino, J.M.; Fiaud, C. Morphology and mechanisms of formation of natural patinas on archaeological Cu-Sn alloys. *Corros. Sci.* **1998**, *40*, 2083–2111. [[CrossRef](#)]
39. Piccardo, P.; Mille, B.; Robbiola, L. Tin and copper oxides in corroded archaeological bronzes. In *Corrosion of Metallic Heritage Artefacts: Investigation, Conservation and Prediction for Long-Term Behaviour*; Dillmann, P., Béranger, G., Piccardo, P., Matthiesen, H., Eds.; European Federation of Corrosion Publication 48; Woodhead Publishing: Cambridge, UK, 2007; pp. 239–262.
40. Oudbashi, O.; Hasanpour, A.; Davami, P. Investigation on corrosion stratigraphy and morphology in some Iron Age bronze vessels by OM, XRD and SEM-EDS methods. *Appl. Phys. A* **2016**, *122*, 262. [[CrossRef](#)]
41. Robbiola, L.; Portier, R. A global Approach to the authentication of ancient bronzes based on the characterization of the alloy-patina-environment system. *J. Cult. Herit.* **2006**, *7*, 1–12. [[CrossRef](#)]
42. Robbiola, L.; Fiaud, C.; Harch, A. Characterization of passive layers of bronze patinas (Cu-Sn Alloys) in relation with tin content of the alloy. In *Modifications of Passive Films, Proceedings of the European Symposium Paris, Paris, France, 15–17 February 1993*, 12th ed.; Marcus, P., Baroux, B., Keddam, M., Eds.; European Federation of Corrosion Publication; The Institute of Materials: London, UK, 1994; pp. 150–154.

43. Robbiola, L.; Fiaud, C. Corrosion structures of long-term burial Cu-Sn alloys: Influence of the selective dissolution of copper. *Editions de la Revue de Métallurgie* **1993**, *6*, 157–162.
44. Robbiola, L.; Fiaud, C.; Pennec, S. New model of outdoor bronze corrosion and its implications for conservation. In Proceedings of the ICOM Committee for Conservation Tenth Triennial Meeting, Washington, DC, USA, 22–27 August 1993; pp. 796–802.
45. Chiavari, C.; Rahmouni, K.; Takenouti, H.; Joiret, S.; Vermaut, P.; Robbiola, L. Composition and electrochemical properties of natural patinas of outdoor bronze monuments. *Electrochim. Acta* **2007**, *52*, 7760–7769. [[CrossRef](#)]
46. Oudbashi, O. Multianalytical study of corrosion layers in some archaeological copper alloy artefacts. *Surf. Interface Anal.* **2015**, *47*, 1133–1147. [[CrossRef](#)]
47. Taube, M.; Davenport, A.; King, A.; Chase, W. Selective dissolution in copper-tin alloys: Formation of corrosion-resistant patina on ancient Chinese bronze mirrors. *MRS Proc.* **1996**, *432*, 283–288. [[CrossRef](#)]
48. Mabilie, I.; Bertrand, A.; Sutter, E.M.M.; Fiaud, C. Mechanism of dissolution of a Cu–13Sn alloy in low aggressive conditions. *Corros. Sci.* **2003**, *45*, 855–866. [[CrossRef](#)]
49. Oudbashi, O.; Hessari, M.; Hasanpour, A.; Shishegar, A. A multianalytical approach for the study on manufacturing process in ancient bronze coffin from Luristan, Western Iran. *Mater. Perform. Charact.* **2017**, *6*, 209–223. [[CrossRef](#)]
50. Scott, D.A. A review of copper chlorides and related salts in bronze corrosion and as painting pigments. *Stud. Conserv.* **2000**, *45*, 39–53.
51. Oudbashi, O. A methodological approach to estimate soil corrosivity for archaeological copper alloy artefacts. *Herit. Sci.* **2018**, *6*, 2. [[CrossRef](#)]
52. Wanhill, R.J.H.; Oudbashi, O. Chapter 12-1B: Fractography of ancient metallic artifacts: Archaeometallurgical fracture analysis and restoration and conservation aspects. In *ASM Handbook Volume 12, Fractography*; ASM International: Materials Park, Novely, OH, USA, to be published in 2022.
53. Hansen, S.; Helwing, B. Die Anfänge der Silbermetallurgie in Eurasien (The beginnings of silver metallurgy in Eurasia). In *Von Baden Bis Troia: Ressourcennutzung, Metallurgie und Wissenstransfer (From Baden to Troy: Use of Resources, Metallurgy and Knowledge)*; Bartleheim, M., Horesj, B., Krauss, R., Eds.; Verlag Marie Leidorf GmbH: Rahden, Germany, 2016; pp. 41–58.
54. Craddock, P. Production of silver across the ancient world. *ISIJ Int.* **2014**, *54*, 1085–1092. [[CrossRef](#)]
55. Conophagos, C.E. Chapter 12 in *Le Laurion Antique et la Technique Grecque de la Production del' Argent (Ancient Laurium and the Greek Technique of Silver Production)*; Ekdotike Hellados: Athens, Greece, 1980; pp. 305–330.
56. Nezafati, N.; Pernicka, E. Early silver production in Iran. *Iran. Archaeol.* **2012**, *3*, 38–45.
57. Gowland, W. Silver in Roman and earlier times: I. Pre-historic and proto-historic times. *Archaeologia* **1918**, *69*, 121–160. [[CrossRef](#)]
58. Gale, N.H.; Stos-Gale, Z.A. Ancient Egyptian silver. *J. Egypt. Archaeol.* **1981**, *67*, 103–115. [[CrossRef](#)]
59. Gale, N.H.; Stos-Gale, Z.A. Lead and silver in the ancient Aegean. *Sci. Am.* **1981**, *244*, 142–152. [[CrossRef](#)]
60. Tylecote, R.F. *The Prehistory of Metallurgy in the British Isles*; The Institute of Metals: London, UK, 1986; pp. 3–4, 54–61.
61. Raub, C.J. The metallurgy of gold and silver in prehistoric times. In *Prehistoric Gold in Europe: Mines, Metallurgy and Manufacture*; Morteani, G., Northover, J.P., Eds.; Kluwer Academic Publishers: Dordrecht, The Netherlands, 1995; pp. 243–259.
62. Tylecote, R.F. *The Early History of Metallurgy in Europe*; Longman: London, UK, 1987; pp. 69–80, 138–140, 280–290.
63. McKerrell, H.; Stevenson, R.B.K. Some analyses of Anglo-Saxon and associated Oriental silver coinage. In *Methods of Chemical and Metallurgical Investigation of Ancient Coinage*; Hall, E.T., Metcalf, D.M., Eds.; Royal Numismatic Society: London, UK, 1972; pp. 195–209.
64. Organ, R.M. The current status of the treatment of corroded metal artifacts. In *NBS Special Publication 479, Corrosion and Metal Artifacts—A Dialogue between Conservators and Archaeologists and Corrosion Scientists*; Brown, B.F., Burnett, H.C., Chase, W.T., Goodway, M., Kruger, J., Pourbaix, M., Eds.; U.S. Department of Commerce/National Bureau of Standards: Washington, DC, USA, 1977; pp. 107–142.
65. Scott, D.A. Technical study of a ceremonial Sicán tumi figurine. *Archaeometry* **1996**, *38*, 305–311. [[CrossRef](#)]
66. Werner, A.E. Two problems in the conservation of antiquities: Corroded lead and brittle silver. In *Application of Science in Examination of Works of Art*; Young, W.J., Ed.; Boston Museum of Fine Arts: Boston, MA, USA, 1965; pp. 96–104.
67. Ravich, I.G. Annealing of brittle archaeological silver: Microstructural and technological study. In Proceedings of the 10th triennial Meeting of the International Council of Museums Committee for Conservation, Washington, DC, USA, 22–27 August 1993; pp. 792–795, Preprints of the Seminar.
68. Wanhill, R.J.H.; Steijaert, J.P.H.M.; Leenheer, R.; Koens, J.F.W. Damage assessment and preservation of an Egyptian silver vase (300–200 BC). *Archaeometry* **1998**, *40*, 123–137. [[CrossRef](#)]
69. Vaníčeková, J.; Děd, J.; Bartuška, P.; Lejček, P. Intergranular failure of Roman silver artefacts. *Mater. Sci. Forum* **2007**, *567–568*, 213–216. [[CrossRef](#)]
70. Vaníčeková, J.; Děd, J.; Bartuška, P.; Drahokoupil, J.; Čerňanský, M.; Lejček, P. Analysis of grain boundaries in an embrittled ancient silver necklace. *Surf. Interface Anal.* **2008**, *40*, 454–457. [[CrossRef](#)]
71. Wanhill, R.J.H.; Hattenberg, T.; Northover, J.P. ESBD of corrosion, deformation and precipitation in the Gundestrup Cauldron. In *Ligas Metálicas: Investigação e Conservação (Metallic Alloys: Research and Conservation)*; Ferreira, A.C., Homem, P.M., Eds.; Faculdade de Letras da Universidade do Porto (Faculty of Letters, University of Porto): Porto, Portugal, 2008; pp. 46–61.
72. Wanhill, R.J.H. Stress corrosion cracking in ancient silver. *Stud. Conserv.* **2013**, *58*, 41–49. [[CrossRef](#)]
73. Garrels, R.M.; Christ, C.L. *Solutions, Minerals, and Equilibria*; Harper and Row: New York, NY, USA, 1965; pp. 379–383.

74. Wanhill, R.J.H.; Hattenberg, T.; Northover, J.P. *Electron Back Scatter Diffraction (ESBD of Corrosion, Deformation and Precipitation in the Gundestrup Cauldron)*; National Aerospace Laboratory NLR Report NLR-TP-2003-490; National Aerospace Laboratory: Amsterdam, The Netherlands, 2003. [\[CrossRef\]](#)
75. Elam, C.F. An investigation of the microstructures of fifteen silver Greek coins (500–300 BC) and some forgeries. *J. Inst. Met.* **1931**, *45*, 57–69.
76. Johnson, W.; Mellor, P.B. *Plasticity for Mechanical Engineers*; D. Van Nostrand Company, Ltd.: London, UK, 1962; pp. 333–334.
77. Wanhill, R.J.H. *Lecture Course on Metallurgy, Embrittlement and Conservation of Ancient Silver: Update 2018*; National Aerospace Laboratory: Amsterdam, The Netherlands, 2018. [\[CrossRef\]](#)
78. Wanhill, R.J.H. Embrittlement of ancient silver. *J. Fail. Anal. Prev.* **2005**, *5*, 41–54. [\[CrossRef\]](#)
79. Sisco, A.G.; Smith, C.S. *Lazarus Ercker's Treatise on Ores and Assaying*; University of Chicago Press: Chicago, IL, USA, 1951; pp. 80–81, 191–198.
80. Thompson, F.C.; Chatterjee, A.K. The age-embrittlement of silver coins. *Stud. Conserv.* **1954**, *1*, 115–126.
81. Smith, C.S. The interpretation of microstructures of metallic artifacts. In *Application of Science in Examination of Works of Art*; Young, W.J., Ed.; Boston Museum of Fine Arts: Boston, MA, USA, 1965; pp. 20–52.
82. Schweizer, F.; Meyers, P. Authenticity of ancient silver objects: A new approach. *MASCA J.* **1978**, *1*, 9–10.
83. Schweizer, F.; Meyers, P. A new approach to the authenticity of ancient silver objects: The discontinuous precipitation of copper from a silver-copper alloy. In Proceedings of the 18th International Symposium on Archaeometry and Archaeological Prospection, Bonn, Germany, 14–17 March 1978; Rheinland-Verlag GmbH: Cologne, Germany, 1979; pp. 287–298.
84. Wanhill, R.J.H. *Archaeological Silver Embrittlement: A Metallurgical Inquiry*; National Aerospace Laboratory NLR Report; NLR-TP-2002-224; National Aerospace Laboratory: Amsterdam, The Netherlands, 2002. [\[CrossRef\]](#)
85. Wanhill, R.J.H. Significance of discontinuous precipitation of copper in ancient silver. *Metallogr. Microstruct. Anal.* **2012**, *1*, 261–268. [\[CrossRef\]](#)
86. Stos-Gale, Z.A.; Gale, N.H. Metal provenancing using isotopes and the Oxford archaeological lead isotope database (OXALID). *Archaeol. Anthropol. Sci.* **2009**, *1*, 195–213. [\[CrossRef\]](#)
87. Stos-Gale, Z.A.; Gale, N.H. The sources of Mycenaean silver and lead. *J. Field Archaeol.* **1982**, *9*, 467–485.
88. Gale, N.H.; Stos-Gale, Z.A. Bronze Age copper sources in the Mediterranean: A new approach. *Science* **1982**, *216*, 11–19. [\[CrossRef\]](#)
89. Weeks, L.; Keall, E.; Pashley, V.; Evans, J.; Stock, S. Lead isotope analyses of Bronze Age copper-base artefacts from al-Midamman, Yemen: Towards the identification of an indigenous metal production and exchange system in the southern Red Sea region. *Archaeometry* **2009**, *51*, 576–597. [\[CrossRef\]](#)
90. Balliana, E.; Aramendia, M.; Resano, M.; Barbante, C.; Vanhaecke, F. Copper and tin isotopic analysis of ancient bronzes for archaeological investigation: Development and validation of a suitable analytical methodology. *Anal. Bioanal. Chem.* **2013**, *405*, 2973–2986. [\[CrossRef\]](#)
91. Radivojević, M.; Roberts, B.W.; Pernicka, E.; Stos-Gale, Z.; Martín-Torres, M.; Rehren, T.; Bray, P.; Brandherm, D.; Ling, J.; Mei, J.; et al. The provenance, use, and circulation of metals in the European Bronze Age: The state of debate. *J. Archaeol. Res.* **2019**, *27*, 131–185. [\[CrossRef\]](#)
92. Rademakers, F.W.; Rehren, T.; Pernicka, E. Copper for the Pharaoh: Identifying multiple metal sources for Ramesses' work-shops from bronze and crucible remains. *J. Archaeol. Sci.* **2017**, *80*, 50–73. [\[CrossRef\]](#)
93. Vander Voort, G.F. *Metallography: Principles and Practice*; ASM International: Materials Park, OH, USA, 1999.
94. Vander Voort, G.F. Metallographic specimen preparation for Electron Backscattered Diffraction, Part I. *Pract. Metallogr.* **2011**, *48*, 454–473. [\[CrossRef\]](#)
95. Vander Voort, G.F. Metallographic specimen preparation for Electron Backscattered Diffraction, Part II. *Pract. Metallogr.* **2011**, *48*, 527–543. [\[CrossRef\]](#)
96. Gasteiger, S.; Eggert, G. How to compare reduction methods for corroded silver finds. In *Metal 2001, Proceedings of the International Conference on Metals Conservation, Santiago, Chile, 2–6 April 2001*; McLeod, I.D., Theile, J.M., Degryny, C., Eds.; Western Australian Museum: Fremantle, Australia, 2004; pp. 320–324.
97. Děd, J.; Šilhová, A. Korozní poškození stříbrných předmětů z archeologických nálezů (Corrosion damage of silver objects from archaeological findings). In *Sborník Konference Konzervátorů a Restaurátorů Plzeň (Proceedings of Conservators and Restorers Pilsen)*; Technical Museum of Brno: Brno, Czech Republic, 2005; pp. 44–48.
98. Profantová, N.; Šilhová, A. K problematice kaptorg v Čechách. Na základě detailního studia hrobu 22 z Klecan II (The problems of kaptorgas in the Czech Republic. On the basis of detailed study of grave 22 from Klecany II). *Památky Archeol.* **2010**, *101*, 283–310.
99. Stawinoga, G. Die Tasse des Khans: Die Restaurierung einer mittelalterlichen Silbertasse (The Khan Cup: The restoration of a mediaeval silver cup). *Arb. für Restaur.* **1997**, *30*, 137–142.
100. Turner-Walker, G. *A Practical Guide to the Care and Conservation of Metals*; Headquarters Administration of Cultural Heritage, Council for Cultural Affairs: Taichung, Taiwan, 2008.
101. Fink, C.G.; Polushkin, E.P. *Microscopic Study of Ancient Bronze and Copper*; Technical Publication No. 693-E; American Institute of Mining and Metallurgical Engineers: New York, NY, USA, 1936.
102. Hamilton, D.L. *Methods of Conserving Archaeological Material from Underwater Sites*; Center for Maritime Archaeology and Conservation, Texas A&M University: College Station, TX, USA, 1999.

103. Oudbashi, O.; Shekofteh, A.; Makhzani, S.; Siapoosh, M. Conservation of metal collection in Ebn-e Sina Museum, Hamedan, Iran: From intervening to preventive approaches. In *YOCOCU 2014, Professionals' Experiences in Cultural Heritage Conservation in America, Europe, and Asia*; Macchia, E., Prestileo, F., Cagno, S., Khalilli, F., Eds.; Cambridge Scholars Publishing: Newcastle upon Tyne, UK, 2016; pp. 189–201.
104. Papapelekanos, A. The critical RH for the appearance of "Bronze Disease" in chloride contaminated copper and copper alloy artefacts. *E-Conserv. Mag.* **2010**, *13*, 43–52.
105. Costa, V. The deterioration of silver alloys and some aspects of their conservation. *Stud. Conserv.* **2001**, *46* (Suppl. 1), 18–34. [[CrossRef](#)]
106. Rodgers, B.A. *The Archaeologist's Manual for Conservation*; Kluwer Academic/Plenum Publishers: Dordrecht, The Netherlands, 2004.
107. Watkinson, D. Preservation of metallic cultural heritage. In *Shrier's Corrosion*, 1st ed.; Elsevier Science: Amsterdam, The Netherlands, 2009; Volume 4, Section 4.43; pp. 3307–3340.
108. Humphrey, B.J. The application of parylene conformal coating technology to archival and artifact conservation. *Stud. Conserv.* **1984**, *29*, 117–123.
109. SCS Parylene Deposition Equipment. 2002. Available online: [www.scscoatings.com](http://www.scscoatings.com) (accessed on 15 June 2021).
110. Wolfram, J.; Brüggerhoff, S.; Eggert, G. Better than Paraloid B-72? Testing Poligen<sup>®</sup> waxes as coatings for metal objects. In *Metal 2010, Proceedings of the Interim Meeting of the ICOM-CC Metal Working Group, Charleston, SC, USA, 11–15 October 2010*; Mardikian, P., Chemello, C., Watters, C., Hull, P., Eds.; International Council of Museums: Paris, France, 2011; pp. 167–177.
111. Paterakis, A.B.; Lafuente, D.; Cano, E. The corrosive influence of acetic acid emissions on bronze and the efficacy of two protective coatings. In *Metal 2010, Proceedings of the Interim Meeting of the ICOM-CC Metal Working Group, Charleston, SC, USA, 11–15 October 2010*; Mardikian, P., Chemello, C., Watters, C., Hull, P., Eds.; International Council of Museums: Paris, France, 2011; pp. 178–184.
112. Elia, E.; Dowsett, M.; Adriaens, A. On the use of alcoholic carboxylic acid solutions for the deposition of protective coatings on copper. In *Metal 2010, Proceedings of the Interim Meeting of the ICOM-CC Metal Working Group, Charleston, SC, USA, 11–15 October 2010*; Mardikian, P., Chemello, C., Watters, C., Hull, P., Eds.; International Council of Museums: Paris, France, 2011; pp. 193–200.
113. Casaletto, M.P.; Cirrincione, C.; Privitera, A.; Basilissi, V. A sustainable approach to the conservation of bronze artworks by smart nanostructured coatings. In *Metal 2016, Proceedings of the Interim Meeting of the ICOM-CC Metal Working Group, New Delhi, India, 26–30 September 2016*; Menon, R., Chemello, C., Pandya, A., Eds.; International Council of Museums: Paris, France, 2016; pp. 144–152.
114. Aufray, M.; Esvan, J.; Balbo, A.; Grassi, V.; Monticelli, C.; Zanotto, F.; Benetti, F.; Sperotto, W.; Tedesco, E.; Bernardi, E.; et al. Protection of outdoor bronzes with eco-friendly and non-hazardous coatings based on silane and fluoropolymers: Results from the B-IMPACT project. In *Metal 2019, Proceedings of the Interim Meeting of the ICOM-CC Metal Working Group, Neuchatel, Switzerland, 2–6 September 2019*; Chemello, C., Brambilla, L., Joseph, E., Eds.; International Council of Museums: Paris, France, 2019; pp. 222–231.
115. Wanhill, R.J.H. Case histories of ancient silver embrittlement. *J. Fail. Anal. Prev.* **2011**, *11*, 178–185. [[CrossRef](#)]